The El Niño Southern Oscillation (ENSO) Recharge Oscillator Conceptual Model : Achievements and Future Prospects

Vialard J.[1], F-F. Jin[2,3], M.J. McPhaden[4], A. Fedorov[5,1], W. Cai[6,7,8,9], S-I. An[10], D. Dommenget[11], X. Fang[12], M.F. Stuecker[13,3], C. Wang[14], A. Wittenberg[15], S. Zhao[2], F. Liu[1], S-K. Kim[16], Y. Planton[11], T. Geng[6,7], M. Lengaigne[17], A. Capotondi[18], N. Chen[19], L. Geng[2], S. Hu[20], T. Izumo[21], J-S. Kug[22], J-J. Luo[23 24], S. McGregor[11], B. Pagli[21], P. Priya[11], S. Stevenson[25], S. Thual[26]

1. LOCEAN-IPSL, IRD-CNRS-MNHN-Sorbonne Universités, Paris, France
2. Department of Atmospheric Sciences, SOEST, University of Hawai‘i at Mānoa, Honolulu, USA
3: International Pacific Research Center (IPRC), SOEST, University of Hawai‘i at Mānoa, Honolulu, USA
4. NOAA/PMEL, Seattle, Washington, USA
5. Department of Earth and Planetary Science, Yale University, New Haven, USA
6. Physical Oceanography Laboratory/Frontiers Science Center for Deep Ocean Multispheres and Earth System/Sanya Oceanographic Institution, Ocean University of China, Qingdao, China
7. Laoshan Laboratory, Qingdao, China
8. State Key Laboratory of Marine Environmental Science & College of Ocean and Earth Sciences, Xiamen University, Xiamen, China
9. State Key Laboratory of Loess and Quaternary Geology, Institute of Earth Environment, Chinese Academy of Sciences, Xi'an, China
10. Yonsei University, Seoul, Republic of Korea.
11. ARC Centre of Excellence for Climate Extremes, School of Earth, Atmosphere and Environment, Monash University, Melbourne, Australia
12. Department of Atmospheric and Oceanic Sciences and Institute of Atmospheric Sciences, Fudan University, Shanghai, China
13. Department of Oceanography, School of Ocean and Earth Science and Technology (SOEST), University of Hawai‘i at Mānoa, Honolulu, USA
14. State Key Laboratory of Tropical Oceanography, South China Sea Institute of Oceanology, Chinese Academy of Sciences, Guangzhou, China
15. NOAA Geophysical Fluid Dynamics Laboratory, Princeton, New Jersey, USA
16. Irreversible Climate Change Research Center, Yonsei University, Seoul, Republic of Korea
17. MARBEC, University of Montpellier, CNRS, IFREMER, IRD, Sète, France
18. University of Colorado Cooperative Institute for Research in Environmental Sciences & NOAA Physical Sciences Laboratory, Boulder, USA
19. Department of Mathematics, University of Wisconsin-Madison, Madison, USA
20. Division of Earth and Climate Sciences, Nicholas School of the Environment, Duke University, Durham, USA
21. UMR 241 SECOPOL (ex-EIO), IRD-IFREMER-ILM- Université de la Polynésie française, Tahiti, French Polynesia
22. School of Earth and Environmental Sciences, Seoul National University, Seoul, Republic of Korea.
23. Institute for Climate and Application Research (ICAR), Nanjing University of Information Science and Technology, Nanjing, China.
24. SKLLQG, Institute of Earth Environment, Chinese Academy of Sciences, Xi'an, China
25. Bren School of Environmental Sciences and Management, University of California at Santa Barbara, Santa Barbara, California
26. Mercator Ocean International, Toulouse, France

Submitted to *Reviews of Geophysics*

24 July 2023

Abstract (239 words, max 250)

The Recharge Oscillator (RO) is a simple mathematical model of the El Niño Southern Oscillation (ENSO). In its original form, it is based on two ordinary differential equations that describe the evolution of equatorial Pacific sea surface temperature and oceanic heat content. These equations make use of physical principles that operate in nature: (i) the air-sea interaction loop known as the Bjerknes feedback, (ii) a delayed oceanic feedback arising from the slow oceanic response to near-equatorial winds, (iii) state-dependent stochastic forcing from intraseasonal wind variations known as westerly wind bursts (WWBs), and (iv) nonlinearities such as those related to deep atmospheric convection and oceanic advection. These elements can be combined in different levels of RO complexity. The RO reproduces ENSO key properties in observations and climate models: its amplitude, dominant timescale, seasonality, and warm/cold phases amplitude asymmetry. We discuss the RO in the context of timely research questions. First, the RO can be extended to account for ENSO pattern diversity (with events that either peak in the central or eastern Pacific). Second, the core RO hypothesis that ENSO is governed by tropical Pacific dynamics is discussed from the perspective of influences from other basins. Finally, we discuss the RO relevance for studying ENSO response to climate change, and underline that accounting for ENSO diversity, nonlinearities, and better links of RO parameters to the long term mean state are important research avenues. We end by proposing important RO-based research problems.

Plain language summary (193 words, max 200)

The El Niño Southern Oscillation (ENSO) is the main driver of Earth's year-to-year climate variations. ENSO arises from air-sea interactions in the tropical Pacific, but influences climate and societies globally. In recent decades, progress in the observing system and in numerical modeling yielded a better understanding of the physical processes that govern ENSO. Such understanding can be encapsulated in the Recharge Oscillator (RO) *conceptual model*, a simple mathematical representation of ENSO fundamental mechanisms, which accounts for ENSO's essential properties: its amplitude, dominant period, tendency to peak at the end of the year, and tendency for larger warm (El Niño) than cold (La Niña) events. We discuss this framework and propose how to adapt it to explore pressing research topics. First, recent research indicates that the RO can be extended to account for the ENSO diverse spatial patterns of ENSO variability, with anomaly centers in either the central or eastern Pacific. Second, we discuss RO applications for studying influences of regions outside the tropical Pacific on ENSO. Finally, we discuss the RO as a tool to understand the ENSO response to climate change. We conclude by compiling important problems related to these challenging topics.

1. Introduction

Why ENSO matters. The El Niño / Southern Oscillation (ENSO) drives the largest fraction of Earth's year-to-year climate variations (e.g. Trenberth 2020). ENSO emerges from the interplay between oceanic and atmospheric dynamics in the tropical Pacific, as originally outlined by Bjerknes (1966, 1969). Teleconnections through the atmosphere transmit ENSO's influences globally (e.g. Taschetto et al. 2020). ENSO therefore affects global temperature extremes, droughts and floods, tropical cyclones, marine and terrestrial ecosystems, fisheries, and agriculture. These changes have worldwide societal, economic, and environmental impacts (McPhaden et al.,2006).

Three decades of progress. The far-reaching impacts of ENSO have spurred advances in observing, modelling, and understanding the phenomenon over the past decades. A basin-scale tropical Pacific observing system was established in the early 1990s (e.g. McPhaden et al. 1998; McPhaden et al. 2020a), and coupled ocean-atmosphere models now reproduce many aspects of observed ENSO dynamics (Guilyardi et al. 2020), allowing skillful dynamical forecasts up to one year ahead (e.g. L'Heureux et al. 2020). Such advances have improved the understanding of many aspects of ENSO (e.g. Timmermann et al. 2018), including the discovery that ENSO's seasonal-to-interannual basin-scale dynamics are low-dimensional, i.e. they can be characterized using a limited number of parameters. This explains why relatively simple mathematical (or conceptual) models can account both qualitatively and quantitatively for key ENSO properties (e.g. Neelin et al. 1998; Wang 2018; Jin et al. 2020).

Challenges and timeliness. Despite this progress, important questions have yet to be addressed. As our planet warms, there is a pressing need to anticipate potential changes in ENSO behavior in a warming world. Early model simulations and projections of the impacts of anthropogenic warming on ENSO yielded diverse outcomes (Collins et al. 2010; Vecchi and Wittenberg 2010; Chen et al. 2017). Subsequent analyses, using refined models capable of replicating the most intense El Niño events, suggest recent (Cai et al. 2023) and future (Cai et al. 2021) increases in the occurrence of extreme ENSO events, with future warm events having a more rapid onset and longer duration (Lopez et al. 2022). Yet, climate model ENSO projections are uncertain (Maher et al. 2022), as they are still impaired by long-standing systematic biases, such as an eastern equatorial Pacific cold tongue that is too cold and extends too far west (e.g. Bellenger et al. 2014). Such biases limit the ability of these models to represent key ENSO dynamics (e.g. Bayr et al. 2019), and extreme El Niño events (Bayr et al. 2024). Quantitative tools linking the mean state of the tropical Pacific to ENSO characteristics would enhance our understanding of the impacts of model biases and climate changes on ENSO. Conceptual models of ENSO can provide such tools.

Brief review of conceptual models. Several ENSO conceptual models were developed in the late 1980s and 1990s. All of these models incorporate the positive feedback proposed by Bjerknes (1966; 1969), wherein equatorial Pacific sea surface temperature (SST) anomalies trigger fast atmospheric and oceanic responses that serve to intensify those SST anomalies over the following months. These models differ, however, in their representation of the delayed negative feedbacks that terminate ENSO events, and can induce transitions between the warm and cold phases of ENSO. The *delayed oscillator* (Suarez and Schopf 1988; Battisti and Hirst 1989) emphasizes reflections of westward-moving near-equatorial oceanic Rossby waves[1] into eastward-moving equatorial Kelvin waves at the western boundary of the Pacific, and the delayed effect of these reflected waves on reversing the temperature anomaly of water that is upwelled into the surface layer of the eastern equatorial Pacific. The seminal work of Wyrtki (1985) and Cane and Zebiak (1985) suggested an important role for the western tropical Pacific subsurface heat content in ENSO phase transitions. Building on that, Jin (1996; 1997ab) proposed the *recharge oscillator* (hereafter RO), which summarizes the time-integrated effects of the subsurface Kelvin and Rossby wave adjustments as a poleward "discharge" or equatorward "recharge" of subsurface heat content, which then affects the cold tongue SST via vertical and zonal advection. The *advective-reflective oscillator* (Picaut et al. 1997) emphasizes reflections of eastward-moving equatorial Kelvin waves into westward-moving off-equatorial Rossby waves at the eastern boundary, and their effects on near-surface zonal currents in the equatorial central Pacific. The *western Pacific oscillator* (Weisberg and Wang 1997; Wang et al. 1999) highlights the role of wind-forced (rather than reflected) equatorial Kelvin waves in the western Pacific in providing a delayed negative feedback. A unified oscillator incorporating all four of these delayed negative feedbacks was proposed by Wang (2001).

Focus on the RO. In this synthesis, we concentrate on the RO for several reasons. First, it explicitly represents oceanic heat content variations, and captures their observed predictive power of ENSO more than one year ahead (e.g., Meinen and McPhaden 2000). The RO's simple equation also implicitly account for oceanic wave reflections that play an important role in both the delayed, and advective-reflective oscillators. The RO has been extended to explicitly include several key ENSO processes (such as nonlinearities, or a representation of random

[1] Equatorial waves are a class of planetary scale wave motions that affect ocean circulation and thermocline depth variations within a few degrees of the equator, and play an important role in understanding ENSO dynamics.

forcing from atmospheric synoptic variability; e.g. Jin and An 1999; Jin et al. 2020), and can quantitatively account for ENSO properties in observations and simulations, as we will showcase in this review. Over the years, the RO has become the leading and simplest unifying conceptual framework to understand ENSO behavior in models and observations.

Purpose. The details of the RO model, and a verification of its core hypotheses, were reviewed by Jin et al. (2020). Here, we remind ENSO basics (section 2), survey the RO ability to encapsulate ENSO mechanisms (section 3) and emulate its key properties (section 4). Based on a detailed literature review, we further discuss desirable RO extensions that are motivated by pressing research questions (section 5). Section 6 synthesizes this review. Section 7 discusses future RO applications in the form of nine important research questions.

2. ENSO in observations and models

2.1. Observed tropical Pacific background climatology

Walker Cell. ENSO variations are conditioned by the background state on which they develop. So, to understand ENSO, we first need to define what we consider to be "normal" in the tropical Pacific (words in italics below refer to the Fig. 1 sketch). Deep atmospheric convection (towering cumulus clouds with heavy precipitation) only occurs above an SST threshold of ~27.5°C (Gadgil et al. 1984; Graham and Barnett 1987), due to the effect of SST on atmospheric stability (Neelin and Held, 1987). The western equatorial Pacific *warm pool* is climatologically warm (> 28°C, Fig. 2a), giving rise to ascending motions, deep convection and mid-tropospheric latent heat release. The eastern equatorial *cold tongue* is below the convective threshold (~24°C, Fig. 1, Fig. 2a), leading to subsidence and low clouds that lose heat to space. The easterly low-level *trade winds* (Fig. 2a) connect the subsident region in the east to ascending motions in the west, with a westerly return flow in the upper troposphere. This atmospheric circulation cell on the equatorial plane is referred to as the *Walker Circulation*, after Sir Gilbert Walker, the early 20th century meteorologist who discovered the atmospheric signature of ENSO known as the Southern Oscillation (Walker, 1924).

Warm pool & cold tongue. The low level *trade winds* apply a westward force on the upper ocean. As a result, sea level rises in the western Pacific and falls in the eastern Pacific to create a counterbalancing zonal pressure gradient force. Changes in sea level are mirrored in the interior ocean by changes in the depth of the *thermocline*, i.e., the sharp vertical temperature gradient that separates the warm surface layer from the cold ocean interior, which shoals in the east and deepens in the west (Fig. 1 vertical section). The deep thermocline in the west results in a subdued cooling of the ocean surface by vertical mixing. The resulting deep warm surface layer is referred to as the western Pacific *warm pool*. Due to the Coriolis force, the trade winds in the eastern Pacific induce an equatorial divergence (poleward wind-driven flow on both sides of the equator) and *upwelling* (ascending motion in the ocean) to feed that divergence. The shallow thermocline in the eastern Pacific facilitates the upwelling transport of cold thermocline water into the surface layer. This process leads to an SST *cold tongue* that extends from the west coast of South America out to the International Date Line (Fig. 1).

Bjerknes feedback. SST contrasts between the cold tongue and warm pool therefore sustain the Walker cell and trade winds, which themselves drive an ocean response that cools the ocean in the east. This positive feedback loop is referred to as the Bjerknes feedback, after Jacob Bjerknes, the Norwegian meteorologist who first described El Niño as a coupled ocean-atmosphere phenomenon (Bjerknes 1966, 1969). Below, we will see that the Bjerknes feedback is an essential element of ENSO dynamics.

Other important structures. Readers can refer to Trenberth (2020) for a description of other important structures of the tropical Pacific mean state. Here, we only focus on those of relevance for the rest of this review. The westward trade winds drive westward ocean surface flow near the equator in the *South Equatorial Current (SEC)*, with a subsurface eastward-flowing current known as the *Equatorial Under-Current (EUC)*. The horizontal shear and density gradients between the cold westward flowing SEC and eastward-flowing warmer water further north is dynamically unstable, leading to the formation of eddy-like *tropical instability waves (TIWs*; Willett et al. 2006*)*. Those prominent westward-propagating undulations of the SST front at the northern edge of the cold tongue at periods of 20-30 days transport heat from the warm NECC to the cold tongue, and vary at the timescale of ENSO, influencing its heat balance in the near-equatorial region (e.g. Vialard et al. 2001).

2.2. Key observed ENSO properties

Amplitude and pattern. Central Pacific SST (Niño-3.4 region, see Fig. 2a) displays SST anomalies of up to 2.5°C during warm ENSO phases and -2°C during cold phases (Fig. 2c). ENSO events are characterized by a warming and enhanced rainfall over most of the central and eastern equatorial Pacific, as well as westerly wind anomalies over the western Pacific (Fig. 2d). The anomalous warming coincides with anomalous surface heat losses to the atmosphere (contours on Fig. 2c). It also shifts deep atmospheric convection eastward (westward during cold events), and the associated heat source or sink triggers a planetary-scale atmospheric response that leads to global climatic impacts (e.g., Taschetto et al. 2020).

Cyclicity and seasonality. The ENSO cycle of warm El Niño and cold La Niña events is irregular, with a return time of same-polarity events anywhere between one and seven years. This is further illustrated by the observed spectrum of average Niño3.4 SST anomalies (hereafter N3.4) that has a broad peak between roughly 3 and 7 years (Fig. 2f) or by the autocorrelation function of N3.4 which indicates a dominant periodicity of about 4 years (Fig. 2g, Jiang et al. 2021). ENSO events usually start growing in late spring and summer, almost always peak at the end of the calendar year (November through January) and generally terminate in the following spring season (Fig. 2g,h). The system then has a tendency to transition to the opposite phase (see, for example, the warm to cold transitions after the 1982, 1986, 1997, 2010 events, Fig. 2c), but can also return to near-neutral conditions (such as after the 2015 strong El Niño), or stay in the same phase for two or more years (e.g. the 1984-1985, 1998-2000, or 2020-22 multi-year La Niña events).

Asymmetry. Figure 2c also reveals asymmetries between warm and cold events. El Niño events tend to be stronger than La Niña events, La Niña events tend to last longer, and warm events are more frequently followed by cold events than the opposite. As will be seen in section 4, there are several reasons for this asymmetry but they all involve nonlinearities in the dynamics of ENSO.

Diversity. The ENSO spatial pattern diversity is another important ENSO characteristic (e.g. Capotondi et al. 2020, Capotondi et al. 2015), which refers to the tendency of ENSO events to have a peak SST anomaly amplitude in the central Pacific (CP events), eastern Pacific (EP events) or anywhere in between. It is revealed through an EOF analysis of the observed tropical Pacific SST anomalies (Fig. 3a). The leading EOF is characterized by a broad central equatorial Pacific warming (Fig. 3a), but the second mode is a dipole that describes a zonal modulation in the position of the SST maximum. Some events peak in the central Pacific (CP type, such as the 2009 CP El Niño, Fig. 3f) and some in the eastern Pacific (EP type, such as the 1997 strong EP and 2006 weak EP El Niño events, Fig. 3c,e). La Niña events tend to display less diverse patterns and to peak in the central Pacific (such as in 1988, Fig. 3d). The nonlinear, boomerang-shaped relation between the first and second principal components (Fig. 3g; Takahashi et al., 2011; Dommenget et al., 2013) implies a strong relation between asymmetries and diversity. Positive and negative PC1 extrema indeed both tend to be associated with positive PC2 values, implying that the strongest El Niño events are both shifted eastward and stronger than the strongest La Niña events. Diversity in the pattern, amplitude, and temporal evolution of ENSO have recently been collectively referred to as ENSO complexity (Timmermann et al. 2018). The standard version of the RO discussed in sections 3, 4 features a single variable for accounting for SST anomalies, and therefore cannot represent ENSO diversity. In section 5, we will discuss recent studies that showcase how the RO can be extended to account for diversity.

2.3. Observed ENSO dynamics

Bjerknes feedback. Figure 4a illustrates the trade wind decrease in the western Pacific in response to warm central and eastern Pacific SST anomalies during 1997. Those westerly anomalies excite downwelling equatorially-trapped Kelvin waves which propagate eastward along the equator, crossing the basin in about 45 days (Fig. 3b). In their wake, they leave eastward current anomalies that push the warm pool edge eastward to the central Pacific, and a depressed thermocline that reduces the upwelling of cool water to the surface in the eastern Pacific cold tongue (Fig. 3b). Those two processes warm the cold tongue. The reduced heat gain from the atmosphere (contours on Fig. 2c) acts as a thermal damping, but is not sufficient to overcome the effects of ocean dynamics. The cold tongue warming feeds back to the atmosphere, further reducing trade wind strength and allowing El Niño to grow: this is the Bjerknes feedback.

State-dependent WWBs. While there is a clear seasonal envelope of trade winds weakening in the central Pacific, it is punctuated by a series of brief episodes of westerly winds (Fig. 3a) lasting a few days to a few weeks, with a zonal span of 1000 to 2000 km. These episodic winds are known as Westerly Wind Events or Bursts (Harrison and Giese 1991; hereafter WWBs). WWBs are often associated with tropical cyclone formation, (Lian et al. 2018) and the convective phases of convectively coupled atmospheric Rossby waves and the Madden-Julian Oscillation (Puy et al. 2016). Fig. 3 illustrates that December 1996 to March 1997 WWBs played an important role in the development of the 1997-98 El Niño (McPhaden, 1999). WWBs are associated with weather events that are not predictable beyond a couple of weeks, and can be seen as a random forcing at the ENSO timescale, and one of the contributors to ENSO irregularity (An et al., 2020a). But while individual WWBs are not predictable, Figure 3a illustrates that they are modulated by ENSO: they can become more frequent and move eastward during warm phases (e.g. Puy et al. 2016). While WWBs occur on a subseasonal time scale and have a strong random component, they provide a critical contribution to the Bjerknes feedback because of their state dependence (Yu and Fedorov 2022).

Tilt and recharge modes. Figure 5 displays an empirical orthogonal function (EOF) decomposition of interannual thermocline depth anomalies in the tropical Pacific, similar to that in Meinen and McPhaden (2000). The leading mode is associated with a tilt of the equatorial thermocline (Fig. 4a), in phase with central Pacific SST anomalies (Fig. 4c,e). During El Niño, central Pacific wind anomalies force downwelling eastward-propagating Kelvin waves that deepen the eastern Pacific thermocline after about 45 days, and westward-propagating upwelling Rossby waves that lift the thermocline up to the western boundary after about 70 days, i.e. almost in phase with SST anomalies. The second mode is more zonally-uniform in sign (Fig. 5b) and is associated with a strong decrease in heat content or discharge during the peak phase of El Niño, and a recharge during the peak phase of La Niña (Fig. 5d,f). This recharge mode is a consequence of the slower equatorial adjustment (after Kelvin and Rossby waves have had the time to reflect at both boundaries, a time scale of at least 7 months), or equivalently to the poleward Sverdrup transport out of the equatorial band during El Niño, and equatorward transport during La Niña (Jin et al. 1997ab). The strong equatorial heat content decline at the end of El Niño and the associated increase in westward currents terminate the zonal and vertical advection anomalies that initiate and drive the event. In many instances the shoaling continues even after the El Niño has ended, producing a large heat content deficit that sets the stage for a follow-on La Niña, as in 1997-1998 (Fig. 4b). This slow heat content discharge (it occurs about 8-10 months after the event was initiated) constitutes the delayed negative oceanic dynamical feedback that terminates the event, sometimes inducing a transition to the opposite phase.

Phase transitions are not systematic due to random WWBs. The ~0.4 correlation coefficient of the recharge mode with the ENSO peak amplitude (Fig. 5d) at ~1 year lead indicates that the western equatorial Pacific oceanic heat content is an ENSO precursor. This was first noted by Wyrtki (1975) and is now used in many statistical forecasts of ENSO since then (e.g Clarke and Van Gorder 2003). A buildup of oceanic heat content is however not a sufficient condition for an El Niño to occur, as for instance in 2014 (McPhaden 2015). This is in part attributable to random differences in WWBs (Puy et al. 2019; McPhaden et al., 2020b). This stochastic element of wind forcing is hence an important ingredient to encapsulate in an ENSO conceptual model.

2.4. ENSO in climate models

Climate models and ENSO. Through an explicit representation of the ocean and atmosphere dynamics and parameterization of their key physical processes, Coupled General Circulation Models (CGCMs) aim to capture the global climate system rich internal or forced variability, including ENSO. In the 1980s and 1990s, CGCMs were only beginning to crudely simulate ENSO (McPhaden et al, 1998; Delecluse et al., 1998). As the CGCMs' resolutions and parameterizations have improved, their ENSO simulations have become more realistic, with better ENSO amplitudes, spectra, spatiotemporal patterns, seasonal timing, inter-event diversity, physical mechanisms, and global teleconnections (Guilyardi et al. 2020; Planton et al. 2021). Some CGCM simulations are now sufficiently realistic to provide close "model-analogs" of observed conditions that, when traced forward in time, yield skillful predictions of ENSO in the real world (Ding et al. 2018). CGCMs can hence be used to perform seasonal forecasts (e.g. L'Heureux et al. 2021), centennial outlooks of ENSO's behavior in a warming world (e.g. Cai et al. 2021), but also help to understand past ENSO variations, characterize its internal variability and extremes, and test hypotheses about ENSO.

CMIP6 database. The climate community coordinates multi-model experiments (Model Intercomparison Projects, or MIPs) including future climate projections (ScenarioMIP; O'Neill et al. 2016), which form one of the bases of the Intergovernmental Panel on Climate Change (IPCC) reports. The last available coupled ocean-atmosphere MIP is CMIP6 (Eyring et al., 2016). Figure 2 showcases the CMIP6 historical simulations ability to reproduce key ENSO features. On average, CMIP6 models have a reasonable ENSO pattern and amplitude (compare panels d,e), spectrum (compare the red and black spectra on Fig. 2f), and tend to peak in winter like observations (black and red seasonally-dependent amplitudes on Fig. 2h). We will come back to persisting ENSO biases in CGCMs below, but overall this figure indicates that CMIP6 offers a collection of CGCM simulations with diverse representations of ENSO characteristics.

RO and CGCMs. Databases like that of CMIP6 offer a great opportunity to test the RO capacity to reproduce ENSO properties in models. Despite CGCMs' wide utility, they are complex, expensive to run, and can be difficult to understand. Conceptual models like the RO have thus emerged as a useful way to understand ENSO in CGCMs and help linking CGCM ENSO biases to errors in high-level physical feedbacks and processes. We will demonstrate the RO capacity to reproduce key ENSO properties in the CMIP6 database in section 4, and discuss the RO usefulness for understanding ENSO biases in section 6.

ENSO biases. Despite progress, many ENSO biases remain in CGCMs (see Guilyardi et al. 2020 and Planton et al. 2021 for reviews). The ENSO amplitude is on average reasonable in CMIP6 (Fig. 2d,e), but some models underestimate and some models overestimate the observed amplitude, offering an opportunity to test the RO ability to explain its main controls (section 4.1). The CMIP6 warming or cooling pattern in models is detached from the South American coast, unlike in observations (Fig. 2d,e). About 80% of CMIP6 models have a dominant ENSO timescale that is too short, with a median dominant period of 42 versus 50 months for observations (Fig. 2g). Approximately 80% of the models display a more cyclic behavior than observations, with a median regularity[2] of 1.5 against 1.3 in observations (Fig. 2g). Models also have a weaker seasonal decrease in ENSO variability than observed during spring (Fig. 2h), *i.e.* they are insufficiently synchronized to the end of the calendar year. CGCM ENSO events also tend to be insufficiently skewed toward warm SSTAs in the cold tongue region (Fig. 2i). Models ENSO SST and winds patterns extend too far in the western Pacific (Figs. 2d,e). The simulated atmospheric responses of equatorial Pacific deep convection, clouds, rain (e.g. Planton et al. 2021), and winds (Figs. 2d,e) to ENSO events are typically too weak. The thermodynamic damping of ENSO SSTAs by air-sea heat fluxes (mainly from cloud shading and evaporative cooling) also tends to be too weak in CGCMs (Fig. 2c,d). This already indicates that two important elements in the Bjerknes feedback are too weak: the destabilizing effect of the wind response to a SST change, and the stabilizing effect of the air-sea flux response to this SST change. Finally, most models underestimate the observed pattern diversity, more specifically the longitudinal range of the maximum SST anomalies at the ENSO peak (Planton et al. 2021).

Mean state biases. Many of these CGCM ENSO biases stem from biases in the simulated background climate, arising from initially small errors in the individual model components that amplify upon coupling. Chief among these CGCM climate biases is the "cold tongue bias", associated with a cold tongue (and the associated dry, subsident regime) that is too strong, and extends too far west (e.g. Bayr et al. 2019; Fig. 2b). Other common biases include: warm SST biases along the coast of South America (Fig. 2b); an excessive "double" ITCZ south of the equator in the east Pacific during boreal spring, with insufficient cross-equatorial southerly winds (Hu and Fedorov 2018; Fig. 2b); a south Pacific convergence zone (SPCZ) in the west Pacific that is too zonally-oriented; and an overly-intense hydrologic cycle (Guilyardi et al. 2020). As discussed in Sec. 5, these background climate biases affect the balance of terms in the mixed layer heat budget, altering key feedbacks that affect ENSO. Beyond the long-term mean climate, CGCMs also struggle to represent other phenomena that affect ENSO's interactions across time scales — including atmospheric intraseasonal variability (Ahn et al. 2017), oceanic tropical instability waves (TIWs) (Ray et al. 2018; Tian et al. 2018; Wengel et al. 2021), the seasonal cycle (Rashid and Hirst 2016), and modes of decadal variability (Power et al. 2017; McGregor et al. 2018).

[2] Regularity is defined in the caption of figure 2, based on the minimum value of the lagged autocorrelation of the Niño3.4 index. A high regularity indicates a more cyclic behavior (i.e. a stronger tendency for an alternation between opposite ENSO phases).

3. Brief RO overview

RO derivation. A full RO derivation and description can be found in Jin et al. (2020): we just give an overview here. In its simplest form, the linear RO (LRO) reduces the evolution of ENSO Sea Surface Temperature *T* and equatorial heat content *h* anomalies to equations 1,2. Jin et al. (1997a) originally used SST anomalies in the eastern Pacific for *T* and western Pacific heat content anomalies for *h* (see Fig. 1 for the usual definition for those two regions). But other regions of strong ENSO signals are often used such as the 5°N-5°S heat content across the entire Pacific (Burgers et al., 2005) or SST anomalies in the Niño3.4 region (e.g. Zhao et al. 2024): we will discuss this in section 7. Equation 1 is obtained through a reduction of the oceanic mixed layer heat budget after assuming simple balance relations between *T*, h, and wind stress, heat fluxes, currents and thermocline depth anomalies (all represented implicitly). Equation (2) for h is obtained through a reduction of equatorial wave dynamics (e.g. Jin et al. 1997b; Fedorov 2010; Table 1 for parameter names and associated physical processes):

$$\frac{dT}{dt} = RT + F_1 h \qquad (1)$$

$$\frac{dh}{dt} = -\varepsilon h - F_2 T \qquad (2)$$

This LRO encapsulates key mechanisms of the Delayed Oscillator (Schopf and Suarez, 1988; Battisti and Hirst, 1989) and advective-reflective oscillator (Picaut et al. 1997) conceptual models of ENSO, as discussed in (Jin 1997ab; Jin and An 1999).

Bjerknes feedback. In equation (1), *R* represents the Bjerknes feedback loop by which SST anomalies can grow. A positive (negative) *R* implies an exponential growth (decay) of *T*. Jin et al. (2020) derive an analytical expression for *R* that is briefly discussed below. Here, we will just briefly summarize the essential physics encapsulated in *R*, which involve a balance between processes that favor a *growth* and processes that favor a *decay* of *T* (Fig. 6; in the rest of the paragraph we describe what happens during an El Niño, but symmetric processes are at work during La Niña). *R* implicitly includes the following positive feedbacks: the thermocline, Ekman and advective feedbacks, respectively associated with remotely and locally-forced downwelling and surface eastward currents, which all induce a warming. There are two main damping mechanisms that contribute negatively to *R*: thermodynamic and dynamic damping. Thermodynamic damping is associated with air-sea fluxes: a positive *T* leads to more clouds and reduced downward shortwave radiation, and to more evaporative cooling through Clausius-Clapeyron. The resulting negative surface net heat flux anomaly (Fig. 2d) damps *T*. Dynamical damping occurs due to the dissipating effect of the mean circulation on *T*: vertical advection will for instance tend to cool a surface-focused warm anomaly by bringing subsurface, cooler water.

Slow equatorial heat content adjustment. The planetary wave dynamics that govern the equatorial oceanic heat content evolution are complex, as they involve waves that have different meridional structures, propagate both eastward (Kelvin waves) and westward (Rossby), at different phase speeds (Rossby waves are slower than Kelvin waves, with a decreasing phase speed for higher order Rossby meridional modes), and reflect at both boundaries (e.g. Boulanger and Menkes 1999). Jin et al. (1997b) however demonstrated that these complex dynamics could be summarized by the simple h equation (2), which can reproduce the observed evolution well (0.89 correlation, Jin et al. 2020), with an ε^{-1} adjustment timescale of ~8-10 months. The $-F_2T_E$ term represents the the effect of the Sverdrup transport on h: a positive T leads to a discharge (*i.e.* $dh/dt < 0$), and negative h at the El Niño peak.

Delayed oceanic feedback. This negative h feedbacks on T through the F_1h term in equation (1), favoring a decrease of T, and a transition to the opposite phase. This represents the effect of a negative h on SST, which is mediated by Rossby wave reflections at the eastern boundary, inducing equatorial westward currents and upwelling in the following months. In the RO, those processes are implicit: they are assumed to be instantaneous, and accounted for by simple balance relations between h and central-eastern Pacific currents and thermocline depth, cooling T through the thermocline (upwelling) and advective (westward currents) feedbacks in relation with a negative h.

BWJ index. Equations 1,2 describe an harmonic oscillator, whose growth rate and period are respectively given by the BWJ index real and complex parts (equation 3, Jin et al., 2006; Lu et al., 2018; Jin et al. 2020). We will see in sections 4.1 and 4.2 that the BWJ index is useful to quantify ENSO amplitude and dominant periodicity in observations and climate models.

$$BWJ = \frac{(R-\varepsilon)}{2} + i\sqrt{F_1F_2 - \frac{(R+\varepsilon)^2}{4}} \qquad (3)$$

Stochastic RO (SRO). The BWJ index real part is negative when estimated from observations or CMIP6 models (i.e. the system is damped, see section 4.1), so that a stochastic forcing is needed to maintain an oscillation, resulting in a ***stochastic RO*** (SRO, within the blue frame in equations 4, 5). The SRO differs from the RO through additional stochastic forcing terms of σ_T, σ_h amplitude in equations 4, 5. Depending on studies, this stochastic forcing is either only added in equation 4, or in both equations 4 and 5, and the ξ_T, ξ_h are either white (uncorrelated in time) or red (correlated in time) noises of unit amplitude. This stochastic forcing mainly represents the effect of WWBs, which heavily influence ENSO evolution (section 2.3), and other synoptic, random (at the ENSO timescale) equatorial Pacific wind stress and heat flux perturbations.

$$\frac{dT}{dt} = RT + F_1 h + \sigma_T \xi_T + \sigma_T \xi_T B H(T) T + bT^2 + cT \quad (4)$$

$$\frac{dh}{dt} = -\varepsilon h - F_2 T + \sigma_h \xi_h \quad (5)$$

Stochastic and deterministic nonlinearities

Linear: LRO
Stochastic: SRO
Non-linear: NRO

Nonlinear RO (NRO). In section 2, we discussed the observed tendency for more WWBs during El Niño (see section 4.4). The $\sigma_T \xi_T B H(T) T$ term (orange frame, where H() is the Heaviside step function) represents this observed WWBs modulation by ENSO, with a larger stochastic forcing amplitude $\sigma_T(1 + BH(T)T)$ for positive T (B > 0), sometimes referred to as "multiplicative noise", or a stochastic nonlinearity. In addition to this stochastic nonlinearity, deterministic nonlinearities (purple frame) can be introduced. Quadratic nonlinearities (bT^2 term) represent physical processes that favor the growth of El Niño relative to La Niña (b > 0), as is the case for the stochastic nonlinearity. The stochastic and quadratic nonlinearities are key to explaining the larger El Niño than La Niña maximum amplitude (section 4.4). Finally, cubic nonlinearities (cT^3 term) represent saturation effects (c < 0), contributing to ENSO amplitude. Those generic quadratic and cubic terms cover various oceanic and atmospheric sources of nonlinearities that will be detailed in section 4.4. Example of symmetry breaking nonlinearities include asymmetries in atmospheric convection response to warm versus cold SST anomalies, or nonlinear oceanic advection (advection of temperature anomalies by current anomalies). Overall, additional terms in the purple and orange frames in equations (4,5) transform the LRO or SRO into a nonlinear RO (hereafter, NRO).

Seasonality. ENSO is a highly seasonal phenomenon, and a seasonal cycle *R(t)* (equation 4) is often assumed to represent ENSO seasonal synchronisation:

$$R(t) = R_0 - R_a \sin(\omega_a t - \varphi) \quad (6)$$

In principle, a seasonality could be introduced in more RO parameters (e.g. F_1, F_2), but we will see in section 4.2 that equation (6) is sufficient to explain observed ENSO seasonality.

Naming conventions and original RO analyses in this review. In the rest of the paper, the linear LRO refers to equations 1,2; the stochastic SRO refers to terms inside the blue frame on equations 4, 5; the nonlinear NRO refers to when any of the terms in the orange or purple frame is included. Finally, we will refer to the *seasonal* LRO, SRO or NRO whenever a seasonal cycle in any of the parameters (such as that of *R(t)* in equation 6) is included. The figures 8-12 original analyses are performed using the SRO or NRO described in the Table 2 caption, whose parameters where obtained from fitting equations 4, 5 to *T, h* time series from observations (table 2 parameter values) or CMIP6 models.

RO representation of ENSO phase changes. The figure 7 sketch summarizes the oscillatory behavior that underpins the RO formulation. During an El Niño, a positive T anomaly grows through the Bjerknes feedback (*RT* term). The associated Sverdrup transport out of the equatorial band depletes *h* through the $-F_2T$ term. The resulting negative F_1h term ($F_1 > 0, h < 0$), representing the combined effect of a shallow thermocline and westward currents, makes *T* decay, eventually terminating the El Niño, leaving the system with a negative *h*. This initiates a negative *T* through the F_1h term, which grows through the Bjerknes feedback (*RT* term). The associated Sverdrup transport into the equatorial band leads to a positive *h*, which favors a positive *T*, re-initiating the cycle. The presence of stochastic forcing of course disrupts this regular cycle, so that the SRO has a slight preference for this succession of phases, but does not always follow it. Finally, the quadratic nonlinearity yields more growth of SST anomalies during El Niño than La Niña (cf section 4.4), and the multiplicative noise forcing leads to a more uncertain evolution of the system in presence of warm anomalies (section 4.5).

RO parameters: analytical approach. RO parameters can be obtained in two different manners. Jin et al. (2020) derive analytical formulae for *R* and F_1 as a function of mean state parameters (such as the temperature horizontal and vertical gradients, mean currents, etc…) and empirical estimates of coupling coefficients (such as the wind stress response per unit of *T*, the coupling coefficients between currents and *h*, etc…). This provides, in principle, a theory for linking the properties of the mean state to the Bjerknes feedback strength. Such a theory is necessary to assess the sensitivity of ENSO characteristics to the mean state, important for understanding the effects of model biases, anthropogenic climate change or long-term natural mean state variations. We will come back to this in sections 5 and 7.

RO parameters: fitting observations or models. The most common way to estimate the RO parameters is however through a multivariate (and potentially nonlinear) fit of equations (1,2) to observed or modelled *T*, *h* time series. Section 4 includes original analyses that demonstrate that this approach leads to ENSO characteristics from the RO that match those in observations and climate model control simulations from the CMIP6 project.

4. How does the RO account for ENSO properties in observations and climate models ?

4.1. Amplitude

Fitted RO captures ENSO amplitude. The study of Vijayeta and Dommenget (2018) showed that fitting an SRO to observations and CMIP3 and CMIP5 models allows to reproduce their ENSO amplitude. Wengel et al. (2018) further investigated the key controls of ENSO amplitude in 35 CMIP5 models, and demonstrated that the R and ε parameters (that control the overall ENSO stability (R-ε)/2) and stochastic forcing amplitude (σ_T, σ_h) jointly explain more than 80% of the ENSO amplitude variance. Figure 8 displays a similar result to that of Wengel et al. (2018), but here obtained using the NRO model and 45 CMIP6 models. Using fitted values (Fig. 2 caption for details) for all the RO parameters allows to explain the observed and CMIP6 ENSO amplitude extremely well (r=0.97, Fig. 8b), with a slight overestimation for larger than observed amplitudes. Only retaining fitted value for the overall ENSO stability (R-ε)/2 and noise amplitude respectively explain 50% and 25% of the ENSO amplitude variance individually (Fig. 8c,d) and 80% together, as in the study of Wengel et al. (2018) (not shown).

Theoretical explanation. Jin et al. (2020) provide a theoretical context to explain those results. They derive an analytical solution for ENSO amplitude in the case of a NRO with no seasonal dependency and *B*=0 and *b*=0 (no multiplicative noise, no symmetry-breaking nonlinearity, just a cubic nonlinearity). In this solution, ENSO amplitude is a function of the stability (R-ε)/2, the stochastic forcing amplitude σ_T, σ_h (and/or the noise decorrelation timescale, with longer timescales also increasing ENSO amplitude), and the cubic nonlinearity parameter *c*. In practice, ENSO amplitude is sensitive to the stability and noise in the vicinity of parameter values derived from observations, but it is weakly sensitive to the cubic nonlinearity parameter *c* for a stable or marginally stable ENSO (Jin et al. 2020). Physically, this can be understood as follows: the cubic nonlinearity acts as a saturation effect and only controls the ENSO amplitude in an unstable case, when a nonlinearity is needed to stop exponential growth. Figure 8a shows that the 45 analyzed CMIP6 models all yield an annual-mean stable growth rate (between -1.6 and -0.2 year^{-1}, with an observed estimate of -0.5), explaining why observed and CMIP6 ENSO amplitude can be accounted for without considering nonlinearities. While one has to bear in mind that the fitted noise can act as a surrogate for incorrectly estimated nonlinearities (such as those associated with the multiplicative noise parameter *B*), this strong convergence of CMIP6 models and observations suggest that ENSO can be viewed as an asymptotically stable (in an annual-mean sense) system driven by noise, whose amplitude grows with noise and/or the system is less damped.

Linking amplitude to mean state. While the above results are a testimony of the RO ability to predict ENSO amplitude, they do not link this amplitude to the mean state, as would be needed to understand ENSO amplitude changes in view of natural or anthropogenically-driven multidecadal Pacific variability (e.g. Power et al. 2021). The RO parameters were indeed obtained by a fit to the model and observed data, but not directly estimated based on their mean state. Kim and Jin (2011) and Kim et al. (2014) have used the BWJ index (Jin et al. 2006) to estimate ENSO stability based on key mean state parameters, as well as parameters describing important ENSO feedbacks (e.g. wind stress – SST coupling or surface heat flux – SST coupling) fitted to models. This approach was successful in explaining ENSO amplitude diversity in 12 CMIP3 models (Kim and Jin 2011), but later failed to explain it in 19 CMIP5 models (Kim et al. 2014). While these two studies succeeded in establishing links between the mean state and some of the key ENSO feedbacks (e.g. thermocline feedback), this was insufficient to establish a clear link between mean state and ENSO amplitude changes under the effect of anthropogenic forcing (Kim and Jin 2011). This points to the need of more research for linking RO parameters with the mean state (section 7). Another difficulty is that coupled models have biased ENSO dynamics, due to compensating biases in the wind stress-SST coupling and thermodynamical damping by air-sea fluxes, which both tend to be underestimated (Kim and Jin 2011; Chene et al. 2021) as a result of the cold tongue bias (Bayr et al. 2019). A lot of CMIP models therefore produce a realistic ENSO amplitude for incorrect reasons.

4.2. Seasonal synchronization

Recipe to ENSO seasonality in the RO. The variance of observed ENSO SST anomalies exhibits a pronounced seasonal cycle, with peak amplitudes in boreal winter (grey bars on Fig 9a-c). Various studies indicate that this fundamental observed ENSO characteristic can be reproduced when including a seasonally-modulated Bjerknes feedback $R(t)$ in the recharge oscillator model (Fig. 9ab, Stein et al. 2010; An and Jin 2011; Stein et al. 2014, Levine and McPhaden, 2015; Dommenget and Yu 2016; Chen and Jin 2020; Jin et al. 2020; Kim and An 2021). Estimating R from a direct fit of the NRO to observations or from the BWJ approach yields positive (unstable) values from July to November with a peak in September (blue curve in Fig. 9a, e.g., Jin et al. 2020; Chen and Jin 2020). Kim and An (2021) provide an approximate analytical solution of the seasonally-dependent ENSO variance, which predicts peak ENSO amplitude ~3 months after the R maximum, i.e. in boreal winter, as observed.

R seasonal modulation mechanisms. The BWJ index allows for a decomposition of seasonal variations of the Bjerknes feedback into contributions from individual oceanic processes (Jin et al. 2020), indicating contributions from many processes, including the thermocline and zonal advective positive feedbacks, dynamical damping by the mean upwelling, or thermodynamical damping (e.g. negative cloud/radiation feedback; Dommenget and Yu 2016). These represent the combined effects of the seasonal changes in climatological background state (zonal and vertical temperature gradients, vertical velocity), the amplitude of the wind stress response to SST anomalies, and the coupling between this wind stress response and the oceanic (i.e., thermocline tilt) response. Further linking the Bjerknes feedback seasonality to well-identified features of the seasonal cycle such as shifts in tropical Convergence zones and the meridional movement of zonal wind anomalies (McGregor et al. 2012, Stuecker et al. 2013, Abellan and McGregor 2016) has so far proven difficult, probably because the R seasonality is a compound effect of many different processes.

RO reproduces ENSO observed seasonality. Using a SRO, Stein et al. (2010) showed that seasonal variations in F_1 play a much weaker role in the ENSO amplitude seasonality than those in R. Figure 9a-c confirms this result: the SRO can reproduce the observed seasonality remarkably well when all the fitted parameters are seasonally-dependent (panel a), or when just the R parameter is seasonally dependent (panel b). Including a seasonal dependence in all the parameters but R yields little seasonality in the ENSO variance, underlining the strong role of the Bjerknes feedback R seasonal dependency.

RO reproduces ENSO seasonality in models. Figure 9d-f further investigates the RO ability to capture the amplitude of the ENSO seasonal cycle in CMIP6 models. Fitting the SRO to individual models allows a very accurate reconstruction of their seasonal amplitude modulation (with an overestimation at larger than observed amplitudes, Fig. 9d). Figures 9e,f indicate that the R seasonality explains half of the inter-model variance, but that, unlike in observations, parameters other than R also contribute to the diversity in the ENSO amplitude seasonal modulation in models. Previous studies have for instance emphasized the role of the F_2 seasonality in models (McGregor et al. 2012, Abellan and McGregor 2016; Izumo et al. 2024). This may be due to the fact that models tend to be in a different dynamical regime than observations. Diagnosing CMIP models using the RO framework for instance suggests a too weak zonal advective feedback seasonality, which can further be related to the cold tongue bias (Chen and Jin 2022).

RO reproduces ENSO predictability spring barrier. It is difficult to discuss ENSO seasonality without referring to the "spring barrier" in predictability, i.e. the tendency for forecasts that are initiated before boreal spring to display much less skill than those initiated after. The lagged autocorrelation of Nino3 SST anomalies as a function of the starting month (Fig. 9a) indicates that persistence forecasts initiated before April-May are much less skillful than those initiated after. This skill decrease is less marked, but nonetheless present, when the ocean subsurface heat content is accounted for in initial conditions (e.g. McPhaden, 2003; Clarke 2014) and in advanced dynamical forecasts (Barnston et al. 2012). Idealized predictability experiments demonstrate that this "spring predictability barrier" is a fundamental characteristic of ENSO, not a property of forecast systems (e.g. Latif et al. 1998). Introducing a Bjerknes feedback seasonal cycle *R(t)* in the SRO and NRO allows reproducing the spring predictability barrier (Fig. 10; Levine and McPhaden 2015). While Levine and McPhaden (2015) emphasized the role of the multiplicative noise forcing for being able to reproduce the spring predictability barrier best, results here indicate that nonlinearities are not needed to reproduce this property (Fig. 10bc). This difference in results can be attributed to the fact that Levine and McPhaden (2015) did not include a linear stochastic forcing nor a $-\varepsilon h$ term in equation (5). Overall, the RO can explain the spring barrier as follows: the RO is stable and noise-driven before spring, and therefore has a poorly predictable evolution at that time. The shift to unstable conditions in summer and fall allows the growth of initial *T*, *h* perturbations to dominate the noise during summer and fall, leading to stronger predictability.

4.3. Dominant timescale

ENSO timescales. ENSO variations display many characteristic timescales: El Niño events typically lasts one year while La Niña tend to last longer (often two, sometimes three years; e.g. Okumura and Deser 2010); the time interval between two warm events is quite variable and up to around ~ 15 years between strong events such as those in 1982-83, 1997-98, and 2015-16 (Fig. 2c). As a result, ENSO indices typically display a broad spectrum with enhanced variance in the 3-7 years band (Fig. 2f). This broad spectral peak is robust, despite the large uncertainties in spectra due to the modulation of ENSO at decadal timescales, even with ~100 years of data (e.g., Wittenberg 2009).

The RO reproduces the broad ENSO spectrum. Early theoretical debates discussed whether ENSO's broad spectrum was typical of a nonlinear phenomenon in the chaotic regime (e.g., Tziperman et al. 1995), or if ENSO could be explained as a damped oscillator excited by weather noise (e.g., Kleeman 2008). Fitting the SRO or NRO to observations (e.g., Jin et al. 2020), CMIP3 and CMIP5 models (e.g., Vijayeta and Dommenget 2018) or CMIP6 models (Fig. 8a) yields a negative annual-mean RO growth rate (R-ε)/2 (section 4.1, although this growth rate becomes seasonally positive, as discussed in section 4.2), and allows to reproduce the overall shape of the ENSO spectrum in observations (Fig. 11a) and CMIP models (Vijayeta and Dommenget 2018). Including an annual cycle in the Bjerknes feedback *R* (section 4.2) leads to enhanced variance on near-annual periodicities (at about ~9 and ~15 months), the so-called combination tones (Stuecker et al. 2013, Stein et al. 2014), as can be seen from a comparison between seasonal and nonseasonal versions of the SRO and observations (Fig. 11a).

The Wyrtki index. The RO theory also provides some tools to estimate the dominant ENSO timescale (central periodicity of the ENSO broad spectral peak), from the complex part of the BWJ index (Eq. 3), which can be approximated as $T_{BWJ}=2\pi/(F_1F_2)^{1/2}$ (Jin et al. 2020). This period is thus inversely related to the delayed oceanic feedback strength (F_1) and to the recharge-discharge efficiency (F_2). Lu et al. (2018) showed that T_{BWJ} computed from fitted RO parameters can explain the diversity of the ENSO dominant period (measured as the ratio of 3-8 to 1-3 years spectral energy) across CMIP5 models and observations. Here, we compare T_{BWJ} to a different metric of the dominant ENSO timescale in CMIP6 models, based on the autocorrelation of the Nino3.4 index (see Fig. 2g caption). The relation between ENSO periodicity and T_{BWJ} is much stronger (R=0.87, Fig. 10b) than that with simpler parameters such as the mean thermocline depth or various properties of the wind stress coupling with SST (R < 0.30, Lu et al. 2018). RO-based diagnostics suggests that climate models have the right ENSO period with wrong dynamics, due compensating errors between a too strong oceanic feedback F_1 and too weak recharge efficiency F_2 (Lu et al. 2018). The RO thus provides useful tools for understanding the controls of ENSO dominant timescales. Yet, T_{BWJ} underestimates the ENSO period in observations and models (slope < 1 on Fig. 10b, yielding an estimated 3 against 4.2 years dominant timescale for observations). This may be related to not accounting for ENSO diversity in the current RO formulation.

4.4. Asymmetries

Nonlinear symmetry-breaking processes. ENSO is asymmetrical: El Niño events tend to be stronger and shorter than La Niña events; strong El Niño events often transition into La Niña, while the opposite is less frequent (An et al. 2020b). Solutions of the SRO are very symmetrical (compare the 0.91 skewness of the observed Nino3 SST with the -0.01 skewness of the SRO solution on Fig. 12ab): nonlinearities are required to break this symmetry (e.g. Jin et al. 2020). Several nonlinearities have been proposed to explain the ENSO asymmetry, some of atmospheric and some of oceanic origin. Atmospheric nonlinearities include the SST threshold for deep convection, which leads to a stronger and eastward-shifted rainfall and wind stress response to positive SST anomalies, relative to negative ones (e.g. Hoerling et al. 1997; Kang and Kug 2002; Frauen & Dommenget, 2010; Choi et al. 2013; Takahashi et al. 2019; Geng et al. 2019; Srinivas et al. 2024). The second source of atmospheric nonlinearity is stochastic, and associated with the more prevalent and eastward-shifted WWBs in presence of positive SST anomalies (section 2.3 and, e.g., Kessler et al. 1995; Lengaigne et al., 2004; Eisenman et al., 2005; Puy et al. 2016; Capotondi et al., 2018). Oceanic nonlinearities include temperature advection, both associated with low-frequency the "Nonlinear Dynamical Heating" (NDH) nonlinear advection terms (e.g. $-u'\partial_x T'$) that enhance the warming during El Niño (e.g. Wang and McPhaden 2000; Jin et al. 2003; An and Jin 2004) and the thermal damping by TIWs that is weaker during El Niño (e.g. Vialard et al. 2001; An et al. 2008). A more efficient thermocline feedback during El Niño has been proposed to contribute to the genesis of strong events (e.g. Timmermann et al. 2003). Finally, some studies attribute ENSO asymmetry to an enhanced oceanic response to western Pacific wind forcing during El Niño (Im et al., 2015; An & Kim, 2017, 2018). We will come back to these very diverse explanations below.

Stochastic nonlinearities in the RO. As described in section 3, the nonlinearity associated with WWBs is represented as a state-dependent stochastic forcing in the NRO (orange frame in equation 4), with B representing the strength of this state-dependency (e.g. Levine and Jin, 2017). Introducing this nonlinear, state-dependent noise forcing in the RO ($B > 0$) leads to larger-amplitude warm events (Jin et al. 2007; Levine et al., 2016; An et al. 2020a; Fig. 12b).

Deterministic nonlinearities in the RO. Various studies have also used the RO to investigate the effect of deterministic nonlinearities. Frauen and Dommenget (2010) demonstrated that coupling the linear oceanic dynamics of the RO to the nonlinear wind stress response to SST provided by an AGCM was sufficient to reproduce the observed ENSO amplitude asymmetry. Takahashi et al. (2019) showed that changing R from a negative (damping) to zero (neutral) value to represent a less-damped system above the threshold for deep atmospheric convection could allow the RO to reproduce strong El Niño events. An (2008) similarly demonstrated that introducing more damping for negative T (interpreted as the asymmetrical effect of TIWs) lead to larger amplitude Niño than Niña. Geng et al. (2019) separately represented oceanic and atmospheric nonlinearities in the RO, by setting different values of R and F_2 depending on the sign of T, and concluded that atmospheric nonlinearities were key to generating ENSO amplitude asymmetry. An et al. (2020a) and Kim et al. (2020) finally demonstrated that introducing nonlinearities in the RO reproduced the observed amplitude asymmetries, and interpreted those nonlinearities as being caused by NDH.

Ambiguous source of RO deterministic nonlinearities. Overall, most studies indicate that introducing non-linear terms allows the RO to account for the observed stronger El Niño than La Niña events (Geng et al. 2019; An et al. 2020a; Kim and An 2020; Dommenget and Al Ansari 2022; compare the NRO to the LRO T skewness on Fig. 12a). It is however not easy to attribute the RO deterministic nonlinearity to a single physical cause, because both atmospheric and oceanic processes lead to terms such as the $b\ T^2$ term (Jin et al. 2020), an extra Th term (An et al. 2020a; Kim and an. 2020) or a term proportional to h^2 (Geng et al. 2019) in equation (1). More work is needed to rank the contributions of various atmospheric and oceanic nonlinear processes to the overall nonlinearity, for instance through budget studies in ocean models, as suggested by Jin et al. (2020). A recent study for instance suggests that various source of oceanic nonlinearities cancel, so that atmospheric ones dominate (Liu et al. 2024).

Deterministic vs stochastic. ENSO amplitude increases weakly, but its skewness strongly increases as parameters controlling deterministic and stochastic nonlinearities are increased (Jin et al. 2020; An et al. 2020a; Fig. 12b), but do deterministic or stochastic nonlinearities contribute most to ENSO asymmetry? Kim and An (2020) found that both contribute, with a stronger role of the deterministic nonlinearity. This is supported by the Fig. 12b that indicates a stronger sensitivity of the skewness to b than to B in the NRO.

Outlook. Several studies have attributed the more systematic phase transition after El Niño events to asymmetries in the amplitude or meridional structure of the wind anomalies and/or their southward migration during the event decay phase (Choi et al. 2013; Im et al. 2015; Planton et al. 2018; Geng et al. 2019; Clarke and Zhang 2019; McGregor et al. 2012, 2022). This leads to an observed more efficient discharge after warm than after cold events. Although some aspects of the ENSO asymmetrical phase transitions are reproduced by the NRO (Geng et al. 2019; An et al. 2020a; Dommenget and Al Ansari 2022), more research is needed to investigate the minimum nonlinear terms and associated processes that would allow to reproduce realistic phase transition asymmetries. El Niño events also tend to feature SST patterns that are shifted east relative to those during La Niña. This type of asymmetry cannot be represented by equations 4, 5, which feature a single variable to describe ENSO SST anomalies. Extensions of the RO that can account for ENSO pattern diversity (section 5.1) however address this shortcoming.

5. The RO to tackle ENSO pressing research topics

5.1. Can the RO account for ENSO pattern diversity?

Geometric approach. The RO uses a single variable T to depict ENSO-related SST variations, and hence cannot depict ENSO diversity (section 2). One tentative way is to replace this variable by one that is nonlinearly related to the central and eastern Pacific SST anomalies, such as the eastern edge of the western Pacific warm pool (Williams and Patricola, 2018). Thual and Dewitte (2023) used this approach, yielding a very similar equation to that of the NRO with a single quadratic nonlinearity, but for warm pool displacements instead of *T*. Equatorial SST variations can then be obtained from the position of the warm pool using a simple geometrical approach. This modified RO model reproduces the main ENSO diversity features without an extra dimension. It however underestimates the pattern diversity (the second EOF pattern only explains 3% of the SST anomalies variance in their model, versus 12% in observations), suggesting the need for additional degrees of freedom.

3-variables NRO. Geng et al. (2020) extended the original RO model by adding an equation for SST variations in the central Pacific (T_C) to that of eastern Pacific SST (T_E). They specified a stronger zonal advective feedback in the central Pacific, and stronger thermocline feedback in the eastern Pacific, as suggested by previous work (Kug et al. 2009; Ren and Jin 2013). Their model also features a wind stress that responds linearly to T_C, but nonlinearly to T_E (due to the SST threshold to trigger deep atmospheric convection) and multiplicative noise forcing that seems to play a significant role in generating ENSO diversity (e.g. Fedorov et al. 2015; Hu et al. 2014). They find that the strength of the deterministic atmospheric nonlinearity plays a key role in controlling both the positive T_E and negative T_C skewness. It also generates a qualitatively similar PC1-PC2 nonlinear relation to that observed (Fig. 13b), therefore reproducing observed ENSO spatial pattern asymmetries (eastward shift of the El Niño SST anomalies relative to those during La Niña).

4 variables or more. Fang and Mu (2018) additionally included a fourth, central Pacific zonal current variable in order to explicitly represent the zonal advective feedback in that region. They demonstrate that increasing the strength of the central Pacific zonal advective feedback decreases the ENSO overall amplitude and period, and leads to more CP events. Chen et al. (2022) further added both stochastic forcing (including state-dependent forcing) and an additional stochastic equation to represent decadal changes in the strength of the Walker Cell, which in turn modulate the zonal advective feedback strength in the central Pacific. This model reproduces many crucial properties of the observed ENSO diversity, including the T_E and T_C spectrums, occurrence frequency of CP and EP events, and main ENSO asymmetries. As the model of Geng et al. (2020), it generates a similar PC1-PC2 relation to that in observations (Fig. 13a), *i.e.* reproduces observed ENSO spatial asymmetries.

Minimal RO for diversity? The above RO extensions suggest that it is possible to produce a baseline ENSO diversity without additional degree of freedoms, by using a surface variable that is nonlinearly related to T_E and T_C (Thual and Dewitte, 2023). More observed ENSO diversity features can nonetheless be obtained by adding additional degrees of freedom, yielding a 3 (Geng et al., 2020), 4 (Fang and Mu, 2018) or 5-dimensional (Chen et al., 2022) version of the RO. Those exploratory studies confirm that adding a T_C variable is a promising avenue to account for ENSO diversity in the RO. More research is however needed to determine the requested minimal physics and dimensionality. The models of Fang and Mu (2018) or Chen et al. (2022) both introduce a new prognostic equation for central Pacific currents, while its value is in principle set from the other RO parameters through the near-equatorial semi-geostrophic balance, indicating that such an equation may not be necessary. ENSO diversity has a strong decadal component, with CP or EP-dominated decades (e.g. Capotondi et al. 2020). Geng et al. (2020) and Chen et al. (2022) obtain such decadal ENSO diversity variations, respectively by imposing changes in the atmospheric nonlinearity or through an additional Walker Cell stochastic variable. However, such decadal ENSO diversity variations can also be observed in a simple with no prescribed decadal variation in either the atmospheric nonlinearity or the background Walker Cell (Geng and Jin, 2023ab). In other words, there is currently little consensus on whether ENSO decadal variations occur at random, or involve physical processes internal to the Pacific, or associated with interactions with the extra-tropics or other tropical basins (Power et al. 2021; Fedorov et al. 2020; Capotondi et al. 2023). Overall, recent research indicates that an extended 3-dimensional NRO is a good candidate to account for ENSO diversity, but that more research is needed in order to determine the minimal essential physics, and explore to which extent it can account for decadal variations in ENSO diversity.

5.2. The influence of regions outside the tropical Pacific

Introduction. The RO is derived on the basis that ENSO is primarily governed by dynamics internal to the tropical Pacific. However, recent studies suggest that SST variability outside of the tropical Pacific affects ENSO (see reviews by Cai et al. 2019; Wang 2019; Kug et al. 2021). These regions outside the tropical Pacific (Fig. 14) include the tropical Indian Ocean (e.g. Yu et al. 2002; Kug et al. 2006; Izumo et al. 2010), tropical and subtropical Atlantic (e.g. Wang et al. 2006; Ham et al. 2013) and subtropical-extratropical Pacific (e.g. Vimont et al. 2001). We review the current state of knowledge on this topic under three working hypotheses: i) ENSO influences other regions, but is not influenced by them; ii) coupled feedbacks between ENSO and other regions contribute to ENSO dynamics, but not to its predictability; iii) other regions can trigger ENSO events and contribute to ENSO predictability.

A null hypothesis. There is an unequivocal influence of ENSO on SST in many regions through atmospheric teleconnections (e.g. Taschetto et al. 2020). Extratropical low-frequency SST variability can largely be explained as being driven by a combination of atmospheric stochastic forcing (i.e. weather, Hasselmann 1976) and remote ENSO forcing (e.g. Alexander et al. 2002). Much of the statistics of climate variability outside of the tropical Pacific – including their SSTs lead/lag correlations with ENSO – are consistent with a one-way forcing of ENSO on other regions (*e.g*. Stuecker et al. 2017, Stuecker 2018, Zhang et al. 2021, Jiang et al. 2021; Stuecker 2023). However, SST anomalies in some oceanic regions lead ENSO with correlations that significantly exceed values expected from this null hypothesis (e.g. Jourdain et al. 2016). Several studies also demonstrated a significant influence on ENSO through sensitivity experiments with numerical models (e.g. Vimont et al. 2001; Dayan et al. 2015).

Other regions influence ENSO. A second hypothesis is therefore that ENSO-driven SST signals in regions such as the tropical Indian Ocean (basin-wide warming or cooling that follows ENSO events; e.g. Xie et al. 2009), induce wind signals over the Pacific that feedback on ENSO, affecting its dynamics (e.g. Kug et al. 2006). Several studies using a variety of tools (the RO, observations, a hierarchy of climate models) for instance indicate that the "Indian Ocean capacitor effect" can either damp (e.g. Jansen et al. 2009) or stimulate (e.g. Dommenget et al. 2006; Dommenget and Yu 2017) variability in the Pacific, and significantly contributes to ENSO phase transition (e.g. Annamalai et al. 2005; Kug and Kang 2006) by enhancing the delayed negative feedback associated with ocean dynamics (Dommenget and Yu 2017). The north Pacific Meridional Mode (Chiang et al. 2004) interactions with ENSO likewise have systematic impacts on its dynamics (Stuecker 2018). In such cases, the SST variations in the remote region are caused by ENSO in the first place, and hence do not yield extra predictability (discussion in Zhang et al. 2021, Jiang et al. 2021 and Jiang et al., 2023). For instance, the Indian Ocean basin mode appears to heavily influence ENSO dynamics but does not contribute to its predictability (Jansen 2009; Frauen and Dommenget 2012). The last working hypothesis is that climate variability independent of ENSO can induce wind changes over the tropical Pacific through atmospheric teleconnections, which can contribute to the evolution of ENSO events or trigger them (e.g. Izumo et al. 2010; Ham et al. 2013). In that case, an ENSO predictability gain is expected from considering these regions, as could for example be the case for the tropical Atlantic (*e.g.* Frauen and Dommenget 2012; Chikamoto et al. 2020).

The RO perspective. The RO has proven a useful tool for studying basin interactions (e.g. Jansen 2009; Frauen and Dommenget 2012; Dommenget and Yu 2017; Jiang et al. 2021; Stuecker 2023). There is growing evidence that interactions with the Indian Ocean "capacitor effect" can contribute to RO dynamics, i.e. that RO parameters are also influenced by the Indian Ocean response to ENSO (Jansen et al. 2009; Frauen and Dommenget 2012; Dommenget and Yu 2017). On the other hand, the tropical Atlantic does not seem to contribute strongly to the

RO parameters (Jansen et al. 2009; Frauen and Dommenget 2012; Dommenget and Yu 2017), but to predictability. The numerous studies that argue for an influence of regions outside the tropical Pacific on ENSO (see reviews by Wang 2019 and Cai et al. 2019) provide a strong support for going beyond the "ENSO rules" null hypothesis mentioned above. There is however a lack of consensus on which of the regions on Fig. 14 have the strongest influence. A recent RO-based study has however made an important step in that direction (Zhao et al. 2024). This study performed ENSO hindcasts with an eXtended RO (XRO) that couples a NRO in the Pacific region with simple representations of climate modes in other regions, which feed back to ENSO. The other modes are modeled as seasonally modulated AR(1) processes driven by a combination of stochastic atmospheric forcing and deterministic remote ENSO forcing (Stuecker et al. 2017). Considering initial SST conditions form other regions strongly enhances ENSO predictability at lead times beyond 1 year, yielding similar scores to those obtained through deep-learning approaches, and outperforming dynamical models (Zhao et al. 2024). This approach further allows a quantification of the dominant sources of ENSO predictability outside the tropical Pacific (Fig. 14), with a dominant contribution from the tropical Indian Ocean, followed by the North Pacific and the tropical Atlantic. Thus, dynamical ENSO predictability as formulated in the RO is augmented by the relatively slow decay of initial conditions (i.e., damped persistence) of the other climate modes that can energize ENSO in the right seasons. This approach provides an interesting research avenue into climate mode interactions and their impact on seasonal predictability.

5.3. ENSO in a warmer world

Mean state changes. Understanding how ENSO responds to anthropogenic forcing is a key research topic. Observations and atmospheric re-analyses indicate a La Niña-like strengthening of the equatorial Pacific zonal SST gradient (i.e. less warming in the east) and Pacific Walker circulation over the last 40 years. (*e.g.* McGregor et al. 2014, Seager et al. 2022, Lee et al. 2022, Wills et al. 2022; Heede and Fedorov 2023b; Watanabe et al. 2024). Over the same period, most CMIP historical runs on the other hand indicate a Walker circulation slowdown and enhanced warming in the east (referred to as El Niño-like), that will intensify in the future (Xie et al. 2010; Cai et al, 2014, 2015; Watanabe et al. 2024). Some models reproduce the observed trends over the historical period, but later produce an "El Niño" like pattern and Walker cell slowdown (e.g. Heede and Fedorov 2023b; Cai et al. 2021; Gopika et al. 2023). However, there is growing evidence that discrepancies between model and observations are not entirely due to internal variability (e.g. Seager et al. 2022, Wills et al. 2022). The large presentday systematic biases in CMIP models (e.g. Planton et al. 2021; section 2.4) may indeed affect the balance of processes that influence the warming pattern (e.g. Luo et al. 2018). Some processes such as the less-efficient evaporative cooling feedback over cold water (e.g. Xie et al. 2010; Zhang and Li. 2014) favor more warming in the east, as in models. Other processes such as the effect of aerosols (Heede et al. 2021) or the transient ocean thermostat mechanism (e.g. Clement et al. 1996; Heede et al. 2020) on the other hand induce a subdued eastern Pacific warming, as observed (see Watanabe et al. 2024 review). The Bjerknes feedback probably amplifies the response (e.g. Knutson and Manabe 1995; Vecchi et al. 2006), whether it's El Niño or La Niña-like. Overall, there is a large uncertainty on future changes in the tropical Pacific zonal SST gradient and circulation, but a more robust projected increase in upper-ocean thermal stratification due to the surface-focused warming (*e.g.* Cai et al. 2018; Carréric et al. 2020). While simple box models can account for some of the CMIP projected changes (Sun and Liu 1996, Liu and Huang 1997, Heede et al. 2020), there is currently no widely-accepted conceptual framework for the tropical Pacific mean state response to climate change.

Observed and projected ENSO changes. Observations and paleo proxies suggest an increase in the variability of both the CP and EP ENSO amplitude since the 1950s (see Cai et al. 2021 for a review). Initial inquiries did not find a consensus for future changes in modelled ENSO (e.g. Collins et al. 2010), but an increase and eastward shift of the rainfall response to ENSO was then highlighted (Cai et al. 2014). Further accounting for the model-dependent position of the ENSO anomaly hotspots and narrowing CMIP to models that best describe ENSO diversity and/or extreme events yields a robust increase in EP and CP SST variability, and more frequent extreme El Niño and La Niña events in the future (Cai et al. 2018, Fredriksen et al. 2020, Shin et al. 2022). The most recent CMIP6 simulations also suggest that ENSO should become stronger across a broad range of climate scenarios (Heede and Fedorov 2023a; Cai et al. 2022). Despite this emerging consensus, the above-mentioned uncertainties in the projected mean state changes by climate models, as well as their unrealistic ENSO dynamics linked to mean-state biases (e.g. Kim and Jin 2011; Bayr et al. 2019; Chen et al. 2021) still undermines the confidence in those projections.

Processes of ENSO changes. Several studies have investigated the factors responsible for the diversity of the projected ENSO changes in CMIP models. Chen et al. (2017) found that changes in the thermocline and advective feedbacks were most associated with ENSO amplitude changes, and interpreted these changes in terms of the mean equatorial upwelling. Zheng et al. (2016) on the other hand found that models with the strongest El Niño-like pattern (warming in the east) produced the most consistent increase in EP SST variability, explaining it by a weakened barrier to deep convection. Cai et al. (2014) on the other hand emphasize that this weakened barrier to convection mostly enhances extreme rainfall, not the SST signature of extreme EP events. Several studies rather emphasize that the enhanced vertical stratification due to the surface-focused mean warming increases air-sea coupling and is the main factor for the increase in ENSO variability (Cai et al. 2018; Carréric et al. 2020; Cai et al. 2021). The theoretical study of Thual et al. (2011) supports the idea that enhanced stratification leads to a more unstable ENSO. Overall, there is no clear consensus on the processes responsible for the robust future increase in ENSO variability in CMIP models.

Using the RO to tackle ENSO changes. Only a few studies have so far used the RO framework to address ENSO changes under global warming. Dommenget and Vijayeta (2019) explain the average change in ENSO variance in 20 CMIP models by fitting an RO model to present and future simulations, but did not identify a clear dominant feedback that could explain the changes. Kim and Jin (2011) used the BWJ index (Eq. 3; Jin et al. 2006, Jin et al. 2020) to explain changes in ENSO amplitude in 12 CMIP3 models. They could explain the amplitude changes in those models, but with a wide variety of processes involved. Heede and Fedorov (2023a) and Ferrett and Collins (2019) on the other hand showed that the BWJ index was not able to predict ENSO amplitude changes in several CMIP6 scenarios. Both studies pointed to the omission of some nonlinearities, such as the convective response to changes in background SST. Heede and Fedorov (2023a) also pointed to the possible effect of future changes in stochastic forcing. Table 3 synthetizes the main points in this section. We will discuss future perspectives for using the RO to investigate the response to climate change in section 7.

6. Synthesis

Review concept. The key idea of this review is that a conceptual model of ENSO should encapsulate important knowledge about its essential physical processes, and be able to make quantitative prediction about its key properties, how they depend upon the tropical Pacific mean state, and therefore be able to explain the effect of model biases or of our changing climate on ENSO. In this review, we argue that the recharge oscillator is able to perform many of those tasks, and underline how it can be improved to answer today's important research questions.

RO & ENSO recipe. The low dimensionality of ENSO allows the RO to represent the system state with two variables, the central or eastern Pacific surface temperature T, and the oceanic heat content h (usually in the western Pacific, or over the entire equatorial Pacific), which represents the ENSO "memory" associated with slow oceanic dynamics. In its simplest form, the linear RO (LRO) key ingredients are the Bjerknes feedback *R* (Fig. 6), which represents the tendency of SST anomalies to self-amplify (or decay) through an ocean-atmosphere feedback loop, and the delayed negative feedback associated with oceanic dynamics. The western Pacific heat content indeed decreases (increases) in response to the westerly (easterly) wind anomalies during El Niño (La Niña), and favors a cooling (warming) that eventually switches the system to the opposite phase (Fig. 7). Fitting the LRO to observations yields an asymptotically stable system, in which variability can be sustained by adding stochastic forcing, yielding the stochastic RO (SRO). This stochastic forcing represents random atmospheric synoptic perturbations known as Westerly Wind Bursts (WWBs). The last level of complexity involves nonlinearities, yielding the nonlinear RO (NRO). One important nonlinearity relates to the state-dependency of WWBs: they are more numerous during El Niño than during La Niña, which is often referred to as multiplicative noise. Various other sources of atmospheric or oceanic nonlinearities can be represented as an extra quadratic (i.e. symmetry-breaking) or cubic (i.e. amplitude-limiting) nonlinearity. The RO parameters can be considered as having a seasonal dependency, yielding, *e.g.*, a seasonal NRO. The RO parameters can either be obtained by fitting the RO to observations, or by using the BWJ index analytical formula (Jin et al. 2020).

Key properties. ENSO core properties include its amplitude, seasonality, dominant timescale, asymmetries, and pattern diversity (some ENSO events have maximum amplitude in the eastern Pacific, and some in the central Pacific). Some forms of the RO can provide quantitative predictions for the first four properties. We tested those quantitative predictions on observations and preindustrial simulations from the CMIP6 database. Fitting the RO to observations and CMIP5/6 models always yield an asymptotically stable system. In this regime, the observed and CMIP6 ENSO amplitudes are mostly controlled by the RO growth rate (BWJ index real part, $(R\text{-}\varepsilon)/2$) and by the stochastic forcing amplitude. Fitting a seasonally-dependent Bjerknes feedback $R(t)$ allows the seasonal RO to reproduce the observed peak ENSO amplitude in boreal winter, as well as the observed "spring predictability barrier". It also yields a reasonable estimate of the ENSO amplitude seasonality in models. ENSO has a broad spectral peak in the 3-7 years band. The BWJ complex part (whose period can be approximated as $2\pi/(F_1F_2)^{1/2}$) is linearly related to ENSO dominant period in observations and CMIP6 models (with a 30% underestimation). The observed positively skewed T distribution can be reproduced by the nonlinear RO, when considering multiplicative noise and symmetry-breaking nonlinearities. Overall, the literature and analyses in this paper demonstrate that the RO can quantitatively predict the most important ENSO properties in observations and CMIP models.

RO and ENSO diversity. The RO presented in equations 4, 5 cannot reproduce ENSO diversity, since it only features one *T* variable to describe ENSO SST signals. Diversity is linked to the spatial asymmetry of ENSO, with a tendency for larger amplitude and eastward-shifted El Niño relative to La Niña events. The RO can be extended to reproduce this property, either by replacing the *T* variable by one that represents the eastern edge of the western Pacific warm pool (Thual and Dewitte 2023) or by having two SST variables for western and eastern Pacific SST anomalies (Chen et al. 2022, Geng et al. 2020). In both cases, introducing a quadratic nonlinearity to the eastern Pacific SST equation is an important ingredient for allowing the RO to shift between CP and EP events. More research is needed to identify a minimal model for ENSO diversity (with the above studies using a total of 3 to 5 state variables), and to clearly identify the key nonlinearity for generating extreme El Niño events (interpreted as that associated with deep atmospheric convection by Geng et al. 2020).

RO and inter-basin interactions. The RO is based on the premises that all the involved dynamics occur within the tropical Pacific. Over the last 10 years, a lot of research has pointed to an influence of other tropical basins and of the midlatitude Pacific on ENSO (see reviews by Wang 2019; Cai et al. 2019; Kug et al. 2020). The RO has proven a useful tool to study the effect of basin interactions with ENSO. ENSO-driven variability in remote regions (e.g. the average Indian Ocean response to ENSO) drives wind signal over the Pacific, that systematically contribute to ENSO dynamics, as revealed from the RO parameter values (e.g. Dommenget and Yu 2017). Such systematic influences have a weak impact on ENSO predictability. SST variability independent of ENSO can on the other hand influence the ENSO evolution through teleconnections, contributing to its predictability but not to its internal dynamics, as could be the case for the tropical Atlantic (e.g. Frauen and Dommenget 2012). A recent study further quantifies the influence of individual basins on ENSO, by coupling a NRO in the Pacific with simple representations of SST variability in other basins (Zhao et al. 2024), concluding that the initial SST states of the Indian Ocean, North Pacific, and tropical Atlantic enhance long-range ENSO predictability.

RO and climate change. We have ended our review with what we believe is one of the outstanding ENSO research question, namely its response to climate change, and discuss the RO relevance for this question. The trust in CMIP ENSO projections is jeopardized by the conflicting equatorial Pacific long-term trends in observations and models, and by the persistent cold-tongue bias and resulting erroneous ENSO dynamics in models. There is however growing evidence based on CMIP models for a pre-2100 increase in both CP and EP events amplitude, associated with more prevalent extreme El Niño and La Niña events (Cai et al. 2018, 2021).

The mechanism of this increase is not fully understood, with some studies pointing at the effect of enhanced vertical stratification, which strengthens ocean-atmosphere coupling; and some to the "El Niño-like" warming pattern, which promotes establishment of convection in the eastern equatorial Pacific. So far, applying the RO or BWJ index to ENSO change has had limited success in identifying a clear mechanism that would be responsible for the projected change.

7. Way forward: nine important research questions about ENSO and the RO

Processes behind RO parameters? The analytical theory for each of the RO parameter summarized by Jin et al. (2020) provides a useful tool for linking these parameters to various physical processes. Yet, some parameters are associated with several distinct physical processes, whose respective contributions are not easily quantified. A good example are quadratic nonlinearities (parameter b), that contribute to ENSO amplitude asymmetry (section 4.4) and diversity (section 5.1). Various oceanic and atmospheric processes have been suggested to contribute to those nonlinearities, but their respective contributions are not well identified. As initially suggested by Jin et al. (2020), heat budgets in ocean general circulation models, or sensitivity experiments such as those of Srinivas et al. (2024) and Liu et al. (2024) should help to better identify processes associated with various RO parameters.

What choice for h? The initial RO theory (Jin et al. 1997ab) and its recent presentation (Jin et al. 2020) specify that the ocean memory parameter h should be the western equatorial Pacific heat content. Yet, inspired by Meinen and McPhaden (2000), a lot of studies since Burgers et al. (2005) instead fit the RO to time series of the Warm Water Volume (WWV), i.e. the oceanic heat content for the entire tropical band. Several studies indicate that this variable contains a fast timescale associated with the Kelvin wave response, that is in principle represented within the Bjerknes feedback term RT (e.g. Neske and McGregor 2018; Izumo et al. 2018), and can be analytically derived from the RO framework (Zhao et al. 2021). Recent work has also suggested a better index for describing ENSO memory, also accounting for southwestern equatorial Pacific heat content (Izumo and Colin 2022), or using the maximum thermal gradient (rather than the 20°C) depth to compute h (Dommenget et al. 2023). Finally, we note that little work has been undertaken since Jin (1997b) for describing the equatorial wave dynamics associated with h adjustment (e.g. respective roles of reflections at both boundaries). We feel that a better understanding of the best choice, timescale and dynamics of the RO h variable is needed.

Minimum RO for diversity and extremes? The only important ENSO property that is not accounted for by the “standard” RO versions described in section 3 is pattern diversity, a property also associated with asymmetry (section 4.4) and the occurrence of occasional extreme EP El Niño events. Adding a central Pacific SST variable T_C and considering nonlinear processes is a promising research avenue for accounting for the observed pattern diversity of ENSO. More research is however needed to develop a minimum model for RO diversity and extremes, with questions such as: i) whether it can predict the different diversity features in CMIP6 models, ii) what the minimum model required is (models with up to 5-dimensions have been proposed), iii) what the key non-linearities are and how they should be formulated. These are particularly urgent questions, considering that resolving ENSO diversity is key to understanding ENSO’s response to climate change (see below).

Cycle or series of events? Kessler (2002) and Philander and Fedorov (2003) wondered if ENSO was a cycle or a series of events. The fundamental idea behind the RO is that of a harmonic oscillator with inherent cyclicity. The idea is supported by a phase-space analysis of ENSO (Dommenget and Al Ansari 2023). There are however multiple lines of evidence that stochastic forcing by WWBs play a key role in triggering and/or amplifying ENSO events, which are consistent with the idea that some events are noise-driven rather than the result of cyclicity. Here, we argue that ENSO sometimes display a cyclic behavior, and sometimes develops under the effect of noise forcing with little influence from the previous event (Philander and Fedorov 2003; Dommenget and Al Ansari 2023). For instance, extreme El Niño events in the observed record (Fig. 2c) are systematically followed by La Niña (often two-years La Niña). The strong cyclic behavior after strong El Niño could be associated with a more efficient recharge process during the peak of extreme El Niño events (Im et al. 2015; Clarke and Zhang 2019; McGregor et al. 2022) whose effects can be incorporated in the RO through a nonlinearity in the recharge process.

RO forecasts? In this review, we evaluated the capacity of the RO to reproduce ENSO key properties, but not its capacity to forecast ENSO. This has so far been done only in a handful of studies (Fang and Chen 2023; Zhao et al. 2024). Zhao et al. (2024) in particular demonstrated that the NRO achieves similar scores to those obtained by state-of-the art initialized coupled general circulation models. In the future, we recommend that extensions or refinements to the RO are tested in terms of their hindcast capacity, including for CP and EP events separately for RO versions with more than one SST variable.

Inter-basin interactions? We saw in section 5.2 that there is ample evidence for other basins influencing ENSO core dynamics and/or contributing to the genesis of ENSO events.

Yet, many climate modes have been proposed to have an influence on ENSO. More quantification of the influences of various climate modes on ENSO are needed, whether they contribute to ENSO predictability (i.e. are independent of ENSO but can contribute to its evolution) or part of ENSO dynamics in a wider sense (i.e. are a response to ENSO that feedbacks on ENSO, with no gain in predictability). The RO has also proven a useful tool to provide a conceptual understanding of basin interactions associated with ENSO (e.g. Dommenget and Yu 2017; Stuecker 2023). Such studies need to be encouraged. Zhao et al. (2024) for instance demonstrated a clear long-range ENSO forecast skill increase from accounting feedbacks from other basins, with influences from the tropical Indian Ocean, North Pacific and tropical Atlantic ocean.

Multidecadal variability? An issue that has been little discussed so far is tropical Pacific natural multidecadal variability (see reviews by Power et al. 2021; Capotondi et al. 2023). This multidecadal variability is seen in many aspects of ENSO, including its amplitude, skewness, pattern diversity, or relation between ocean heat content and El Niño. There are two ways to consider this decadal variability: i) as being the result of changes in ENSO dynamics associated with the mean state modulation (that mean state modulation being potentially due to long-memory processes such as the oceanic tunnel to mid latitude, e.g. Fedorov et al. 2020); ii) as being the result of stochastic forcing, with no underlying changes in ENSO dynamics or memory effects (e.g. Wittenberg et al. 2014). Kim and An (2020) for instance demonstrated that decadally-varying RO parameters did allow the RO to reproduce observed decadal changes in ENSO amplitude and skewness, providing some support for i). The NRO with stochastic forcing can on the other hand serve as a good null hypothesis based on ii).

RO parameters from mean state? The analytical theory for the linear RO parameters (Jin et al. 2020) allows linkage between those parameters and the tropical Pacific mean state. It is limited, however, by: i) the fact that it does not yet account for nonlinearities, and ii) it relies on empirical estimates of some coupling parameters that may themselves depend on the mean state (e.g. coupling between the thermocline depth and surface temperature anomalies, wind stress-SST coupling, etc.). This limits the usefulness of this theory for explaining the effect of model biases or of mean states under different climates on ENSO properties. More work is thus needed on a more complete theory of the RO parameter values and underlying processes. In addition to theoretical work, we also suggest to use artificial intelligence methods to obtain nonlinear relations between the RO parameters and mean state descriptors based on the large databases provided by CMIP simulations.

ENSO in a warmer world? A key research question about ENSO is its response to climate change (section 5.3, Table 3). This is a challenging question because of uncertainties in: i) the tropical Pacific mean state future evolution; ii) ENSO dynamics; and iii) ENSO projections in climate models. There are several possible RO-based research avenues. Considering ENSO diversity, and more specifically extreme El Niño events, is key for identifying a robust increase in ENSO amplitude in climate models (Cai et al. 2021). This suggests that a RO model that resolves extreme El Niño events and ENSO diversity, and includes the associated nonlinearities would be a better tool to explain the ENSO future evolution in climate models. Another perspective is to investigate the RO sensitivity to two key features of the response to climate change in observations and models: the change in the zonal SST gradient (which decreases in most models, but has increased over the last decades in observations) and the increase in vertical stratification (identified as a key driver by Cai et al. 2021). A third way forward is to develop tools that can link the RO parameters with the mean state (previous paragraph). The last, most ambitious, goal would be to develop a conceptual model that can also account for the tropical Pacific mean state, and its response to climate change.

Community RO model. One of the tasks that the ENSO conceptual model working group will soon undertake is to publish a technical paper on the RO technical implementation and numerics, along with a RO code distribution in python. This distribution will include the LRO, SRO, and NRO as described in the current article and Jin et al. (2020), including seasonally-dependent versions, and parameter values from fits to various observational products and CMIP6 models. This is not a research question, but certainly an important undertaking for fostering a better use of this powerful tool by the community, and for teaching ENSO dynamics.

Acknowledgements. Most authors of the review are members of the CLIVAR (Climate and Ocean -Variability, Predictability, and Change) Pacific Region Panel working group on conceptual models of ENSO. This group of ~20 ENSO experts met through videoconferences in 2021-22 and during a CLIVAR workshop in Melbourne, Australia in February 2023. This review is one of the achievements of that working group. We acknowledge the logistical and financial support from the CLIVAR International Project Office. JV was supported by the French Agence Nationale pour la Recherche (ANR) ARiSE grant (ANR-18-CE01-0012). MFS was supported by the NSF grant AGS-2141728. This is an IPRC publication X and SOEST contribution Y. NC is grateful to acknowledge the support of the Office of Naval Research (ONR) N00014-24-1-2244.

Data availability statement. Analyses and figures in this paper rely on publicly available data sources. They include ORAS5 re-analysis (Zuo et al. 2019; DOI: 10.24381/cds.67e8eeb7); Tropflux (Praveen Kumar et al. 2012, 2013; available from https://incois.gov.in/tropflux/); HadiSST (Rayner et al. 2003; available from https://www.metoffice.gov.uk/hadobs/hadisst/), and Globcurrent (Rio et al. 2014; https://doi.org/10.48670/mds-00327) data. Historical simulations from the CMIP6 project (Eyring et al. 2016) are available from https://aims2.llnl.gov/search/cmip6. Figure 13 uses simulations with the 3+ boxes RO models from Chen et al. (2022) and Geng et al. (2020).

References

Abellán, E., & McGregor, S. (2016). The role of the southward wind shift in both, the seasonal synchronization and duration of ENSO events. *Climate Dynamics*, *47*(1), 509–527. https://doi.org/10.1007/s00382-015-2853-1

Alexander, M. A., I. Bladé, M. Newman, J. R. Lanzante, N. Lau, and J. D. Scott, 2002: The Atmospheric Bridge: The Influence of ENSO Teleconnections on Air–Sea Interaction over the Global Oceans. J. Climate, 15, 2205–2231, https://doi.org/10.1175/1520-0442(2002)015<2205:TABTIO>2.0.CO;2.

An, S-I., S-K Kim, and A Timmermann, 2020a: Fokker-Planck dynamics of the El Niño-Southern Oscillation. *Scientific Reports*, 10, 16282, https://doi.org/10.1038/s41598-020-73449-7.

An, S. I., Tziperman, E., Okumura, Y. M., & Li, T. (2020b). ENSO irregularity and asymmetry. *El Niño Southern Oscillation in a changing climate*, 153-172.

An, S.-I. (2008). Interannual variations of the tropical ocean instability wave & ENSO. *Journal of Climate*, *21*, 3680–3686. https://doi.org/10.1175/2008JCLI1701.1

An, S.-I., & F.-F. Jin (2011) Linear solutions for the frequency and amplitude modulation of ENSO by the annual cycle, Tellus, 63A, 238-243.

An, S.-I., & Jin, F.-F. (2004). Nonlinearity & asymmetry of ENSO. *Journal of Climate*, *17*, 2399–2412.

Barnston, A. G., Tippett, M. K., L'Heureux, M. L., Li, S., & DeWitt, D. G. (2012). Skill of real-time seasonal ENSO model predictions during 2002–11: Is our capability increasing?. Bulletin of the American Meteorological Society, 93(5), 631-651.

Battisti, D. S., & A. C. Hirst (1989). Interannual variability in the tropical atmosphere-ocean model: influence of the basic state, ocean geometry and nonlineary. *J. Atmos. Sci*., 45, 1687-1712.

Bayr, T., C. Wengel, M. Latif, D. Dommenget, J. Lübbecke, and W. Park, 2019: Error compensation of ENSO atmospheric feedbacks in climate models and its influence on simulated ENSO dynamics. Climate Dyn., 53, 155–172. https://doi.org/10.1007/s00382-018-4575-7

Bayr, T., J.F. Lübbecke, J. Vialard and M. Latif 2024: Equatorial Pacific Cold Tongue Bias Degrades the simulation of ENSO Asymmetry in Climate Models**,** submitted to Journal of Climate

Bjerknes, J. (1966). A possible response of the atmospheric Hadley circulation to equatorial anomalies of ocean temperature. Tellus, 18, 820–829.

Bjerknes, J. (1969). Atmospheric teleconnections from the equatorial Pacific. Mon. *Weather Rev*., 97, 163-172.

Burgers, G., Jin, F.-F., & Oldenborgh, G. J. van. (2005). The simplest ENSO recharge oscillator. *Geophysical Research Letters*, *32*(13). https://doi.org/10.1029/2005GL022951

Cai, W., G. Wang, A. Santoso, M.J. McPhaden, L. Wu, F.-F. Jin, A. Timmermann, M. Collins, G. Vecchi, M. Lengaigne, M.H. England, D. Dommenget, K. Takahashi, and E. Guilyardi, 2015: Increasing frequency of extreme La Niña events induced by greenhouse warming. Nature Climate Change, 5, 132-137, doi: 10.1038/nclimate2492.

Cai, W., S. Borlace, M. Lengaigne, P. van Rensch, M. Collins, G. Vecchi, A. Timmermann, A. Santoso, M. J. McPhaden, L. Wu, M. England, E. Guilyardi, and F.-F. Jin, 2014: Increasing frequency of extreme El Niño events due to greenhouse warming. Nature Climate Change, 4, 111–116. doi:10.1038/nclimate2100.

Cai, W., Santoso, A., Collins, M. et al. Changing El Niño–Southern Oscillation in a warming climate. Nat Rev Earth Environ 2, 628–644 (2021). https://doi.org/10.1038/s43017-021-00199-z.

Cai, W., Wu, L., Lengaigne, M., Li, T., McGregor, S., Kug, J. S., ... & Chang, P. (2019). Pantropical climate interactions. Science, 363(6430).

Cai, W., Ng, B., Wang, G. *et al.* Increased ENSO sea surface temperature variability under four IPCC emission scenarios. *Nat. Clim. Chang.* **12**, 228–231 (2022).

Cai, W., Ng, B., Geng, T., Jia, F., Wu, L., Wang, G., ... & McPhaden, M. J. (2023). Anthropogenic impacts on twentieth-century ENSO variability changes. *Nature Reviews Earth & Environment*, 1-12.

Cane, M. A., & Zebiak, S. E. (1985). A Theory for El Niño and the Southern Oscillation. *Science*, *228*(4703), 1085–1087. https://doi.org/10.1126/science.228.4703.1085

Capotondi et al., 2015: Understanding ENSO diversity. Bull. Amer. Meteor. Soc., 96, 921-938, doi:10.1175/BAMS-D-13-00117.1.

Capotondi, A., P. D. Sardeshmukh, and L. Ricciardulli, 2018: The nature of the stochastic wind forcing of ENSO. J. Climate, 31, 8081-8099.

Capotondi, A., Wittenberg, A. T., Kug, J. S., Takahashi, K., & McPhaden, M. J. (2020). ENSO diversity. El Niño Southern Oscillation in a changing climate, 65-86.

Capotondi, A., McGregor, S., McPhaden, M. J., Cravatte, S., Holbrook, N. J., Imada, Y., ... & Xu, T. (2023). Mechanisms of tropical Pacific decadal variability. *Nature Reviews Earth & Environment*, 1-16.

Chen C, Cane MA, Wittenberg AT, Chen D (2017) ENSO in the CMIP5 simulations: life cycles, diversity, and responses to climate change. J Clim 30:775–801. https://doi.org/10.1175/ jcli-d-15-0901.1.

Chen, H.-C., & Jin, F.-F. (2020). Fundamental behavior of ENSO phase locking. *J. Climate*, *33*, 1953–1968. https://doi.org/10.1175/JCLI-D-19-0264.1

Chen, H.-C., & Jin, F.-F. (2022). Dynamics of ENSO phase-locking and its biases in climate models. *Geophysical Research Letters*, 49, e2021GL097603. https://doi.org/10.1029/2021GL097603

Chen, M., Li, T., Shen, X., & Wu, B. (2016). Relative roles of dynamic and thermodynamic processes in causing evolution asymmetry between El Niño and La Niña. *Journal of Climate, 29,* 2201–2220. https://doi.org/10.1175/JCLI-D-15-0547.1

Chen, N., & Fang, X. (2022). A Simple Multiscale Intermediate Coupled Stochastic Model for El Niño Diversity and Complexity. arXiv preprint arXiv:2206.06649.

Chiang, JCH, and Vimont, DJ. Analogous Pacific and Atlantic meridional modes of tropical atmosphere–ocean variability. J. Climate 2004; **17**: 4143–4158.

Chikamoto, Y., Z.F. Johnson, S.-Y. Simon Wang, M.J. McPhaden, and T. Mochizuki, 2020: El Niño Southern Oscillation evolution modulated by Atlantic forcing. *J. Geophys. Res., 125*, e2020JC016318. https://doi.org/10.1029/2020JC016318.

Choi, K. Y., Vecchi, G. A., & Wittenberg, A. T. (2013). ENSO transition, duration, & amplitude asymmetries: Role of the nonlinear wind stress coupling in a conceptual model. *Journal of Climate*, *26*, 9462–9476. https://doi.org/10.1175/JCLI-D-13-00045.1

Clarke, A. J., S. Van Gorder, Improving El Niño prediction using a space-time integration of Indo-Pacific winds and equatorial Pacific upper ocean heat content, Geophys. Res. Lett., 30(7), 1399, doi:10.1029/2002GL016673, 2003.

Clarke, A. J., & Zhang, X. (2019). On the physics of the warm water volume and El Niño/La Niña predictability. Journal of Physical Oceanography, 49(6), 1541-1560.

Clarke, A. J. (2014). El Niño physics and El Niño predictability. *Annu. Rev. Mar. Sci*, *6*(1), 79-99.

Clement, A. C., Seager, R., Cane, M. A. & Zebiak, S. E. An ocean dynamical thermostat. J. Clim. 9, 2190–2196 (1996).

Collins M, et al (2010): The impact of global warming on the tropical Pacific Ocean and El Niño. Nat Geosci 3:391–397. https://doi. org/10.1038/ngeo868.

Dayan H, Izumo T, Vialard J, Lengaigne M, Masson S (2015) Do regions outside the tropical Pacific influence ENSO through atmospheric teleconnections? Clim Dyn 45:583–601.

Delecluse, P., Davey, M. K., Kitamura, Y., Philander, S. G. H., Suarez, M., and Bengtsson, L. (1998), Coupled general circulation modeling of the tropical Pacific, J. Geophys. Res., 103(C7), 14357– 14373, doi:10.1029/97JC02546.

Ding, H., Newman, M., Alexander, M. A., & Wittenberg, A. T. (2018). Skillful climate forecasts of the tropical Indo-Pacific Ocean using model-analogs. Journal of Climate, 31(14), 5437-5459.

Dommenget D, Yu Y. (2017): The effects of remote SST forcings on ENSO dynamics, variability and diversity. Clim Dyn. 2017;49:2605–24.

Dommenget, D. & Vijayeta, A. (2019): Simulated future changes in ENSO dynamics in the framework of the linear recharge oscillator model. Clim. Dyn. 53, 4233–4248.

Dommenget, D., Priya, P., & Vijayeta, A. (2023). ENSO phase space dynamics with an improved estimate of the thermocline depth. *Climate Dynamics*, *61*(11), 5767-5783.

Dommenget, B. D., & Al-Ansari, M. (2023). Asymmetries in the ENSO phase space. *Climate Dynamics*, *60*(7), 2147-2166.

Dommenget, D., & Yu, Y. (2016). The seasonally changing cloud feedbacks contribution to the ENSO seasonal phase-locking. *Climate Dynamics*, *47*(12), 3661–3672. https://doi.org/10.1007/s00382-016-3034-6

Dommenget, D., V. Semenov, and M. Latif (2006), Impacts of the tropical Indian and Atlantic Oceans on ENSO, Geophys. Res. Lett., 33, L11701, doi:10.1029/2006GL025871.

Eisenman, I., Yu, L., & Tziperman, E. (2005). Westerly wind bursts: ENSO's tail rather than the dog?. Journal of Climate, 18(24), 5224-5238.

Fang, X., & Chen, N. (2023). Quantifying the predictability of ENSO complexity using a statistically accurate multiscale stochastic model and information theory. *Journal of Climate*, *36*(8), 2681-2702.

Fedorov, A. V. (2010). Ocean Response to Wind Variations, Warm Water Volume, and Simple Models of ENSO in the Low-Frequency Approximation. *Journal of Climate*, *23*(14), 3855–3873. https://doi.org/10.1175/2010JCLI3044.1

Fedorov, A., S. Hu, A. T. Wittenberg, A. Levine, and C. Deser, 2020: ENSO low-frequency modulations and mean state interactions. Chapter 8 of: *El Niño Southern Oscillation in a Changing Climate*, American Geophysical Union, Washington, DC, pp. 173-198. https://doi.org/10.1002/9781119548164.ch8

Fedorov, A. V., Hu, S., Lengaigne, M., & Guilyardi, E. (2015). The impact of westerly wind bursts and ocean initial state on the development, and diversity of El Niño events. Climate Dynamics, 44, 1381-1401.

Ferrett, S. and Collins, M., 2019. ENSO feedbacks and their relationships with the mean state in a flux adjusted ensemble. Climate Dynamics, 52, pp.7189-7208.

Frauen C, Dommenget D (2012) Influences of the tropical Indian and Atlantic Oceans on the predictability of ENSO. Geophys Res Lett 39: L02706.

Frauen, C., & Dommenget, D. (2010). El Niño and la Niña amplitude asymmetry caused by atmospheric feedbacks. *Geophysical Research Letters*, *37*, 1–6. https://doi.org/10.1029/2010GL044444

Fredriksen, H.-B., Berner, J., Subramanian, A. C., & Capotondi, A. (2020). How does El Niño–Southern Oscillation change under global warming—A first look at CMIP6. Geophysical Research Letters, 47, e2020GL090640. https://doi.org/ 10.1029/2020GL090640

Gadgil, S., Joseph, P. V., & Joshi, N. V. (1984). Ocean–atmosphere coupling over monsoon regions. Nature, 312(5990), 141-143.

Geng, T., Cai, W., Wu, L., & Yang, Y. (2019). Atmospheric convection dominates genesis of ENSO asymmetry. Geophysical Research Letters, 46, 8387–8396. https://doi.org/10.1029/2019GL083213

Geng, T., Cai, W., & Wu, L. (2020). Two types of ENSO varying in tandem facilitated by nonlinear atmospheric convection. Geophysical Research Letters, 47, e2020GL088784. https://doi.org/10.1029/2020GL088784

Geng, L., & Jin, F.-F. (2023a). Insights of ENSO Diversity from an Intermediate Coupled Model. Part I: Uniqueness and Sensitivity of the ENSO Mode. *Submitted*.

Geng, L., & Jin, F.-F. (2023b). Insights of ENSO Diversity from an Intermediate Coupled Model. Part II: Role of Nonlinear Dynamics and Stochastic Forcing. *Submitted*.

Graham, N. E., & Barnett, T. P. (1987). Sea surface temperature, surface wind divergence, and convection over tropical oceans. Science, 238(4827), 657-659.

Guilyardi, E., A. Capotondi, and M. Lengaigne, S. Thual, and A. T. Wittenberg, 2020: ENSO modeling: History, progress, and challenges. In "El Niño Southern Oscillation in a Changing Climate", American Geophysical Union, Washington, DC, pp. 201-226. https://doi.org/10.1002/9781119548164.ch9

Ham, Y.-G., J. S. Kug, and J.-Y. Park, 2013: Two distinct roles of Atlantic SSTs in ENSO variability: North Tropical Atlantic SST and Atlantic Niño. Geophys. Res. Lett., 40, 4012-4017.

Heede, U.K., A.V. Fedorov, and N.J. Burls. 2020. 'Timescales and Mechanisms for the Tropical Pacific Response to Global Warming: A Tug of War between the Ocean Thermostat and Weaker Walker'. Journal of Climate, April. https://doi.org/10.1175/JCLI-D-19-0690.1.

Heede, U.K., and Fedorov, A.V., 2021: Eastern equatorial Pacific warming delayed by aerosols and thermostat response to CO_2 increase. *Nature Climate Change 11,* 696–703.

Heede, U.K. and Fedorov, A.V., 2023a. Towards understanding the robust strengthening of ENSO and more frequent extreme El Niño events in CMIP6 global warming simulations. Climate Dynamics, 61(5), pp.3047-3060.

Heede, U.K., and Fedorov, A.V., 2023b: A stronger Walker circulation and colder eastern equatorial Pacific in the early 21st century: separating the forced response of the climate system from natural variability. *GRL,* e2022GL101020.

Hu, S., & Fedorov, A. V. (2018). Cross-equatorial winds control El Niño diversity and change. Nature Climate Change, 8(9), 798-802.

Im, S.-H., An, S.-I., Kim, S. T., & Jin, F.-F. (2015). Feedback processes responsible for El Niño-La Niña amplitude asymmetry. *Geophysical Research Letters*, *42*, 5556–5563. https://doi.org/10.1002/2015GL064853

Izumo T, Vialard J, Lengaigne M, et al (2010) Influence of the state of the Indian Ocean Dipole on the following years El Niño. Nat Geosci 3:168–172.

Izumo, T., & Colin, M. (2022). Improving and harmonizing El Niño recharge indices. Geophysical Research Letters, 49, e2022GL101003. https://doi.org/10.1029/2022GL101003

Izumo, T., Colin, M., Jin, F. F., & Pagli, B. (2024). The hybrid Recharge Delayed Oscillator: a more realistic El Niño conceptual model. Journal of Climate, 37(9), 2765-2787.

Jansen MF, Dommenget D, Keenlyside N (2009) Tropical atmosphere - Ocean interactions in a conceptual framework. J Clim 22:550–567.

Jiang, F., Zhang, W., Jin, F.-F., Stuecker, M. F., & Allan, R. (2021). El Niño pacing orchestrates inter-basin Pacific-Indian Ocean interannual connections. Geophysical Research Letters, 48, e2021GL095242. https://doi.org/10.1029/2021GL095242.

Jin, F. F., & An, S. I. (1999). Thermocline and zonal advective feedbacks within the equatorial ocean recharge oscillator model for ENSO. *Geophysical research letters*, *26*(19), 2989-2992.

Jin, F. F., Chen, H. C., Zhao, S., Hayashi, M., Karamperidou, C., Stuecker, M. F., Xie, R., and Geng, L. 2020: Simple ENSO models, in: El Niño Southern Oscillation in a Changing Climate, edited by: McPhaden, M. J., Santoso, A., and Cai, W., Geophysical Monograph Series, AGU, 119–151.

Jin, F. F., Kim, S. T., & Bejarano, L., 2006: A coupled-stability index for ENSO. Geophysical Research Letters, 33.

Jin, F.-F. (1997a). An equatorial ocean recharge paradigm for ENSO. Part I: conceptual model. *Journal of the Atmospheric Sciences*, *54*, 811–829. https://doi.org/10.1175/1520-0469(1997)054<0811:aeorpf>2.0.co;2

Jin, F. F. (1997b). An equatorial ocean recharge paradigm for ENSO. Part II: A stripped-down coupled model. Journal of the Atmospheric Sciences, 54(7), 830-847.

Jin, F.-F., S. T. Kim, and L. Bejarano (2006), A coupled-stability index for ENSO, Geophys. Res. Lett., 33, L23708, doi:10.1029/2006GL027221.

Jin, F.-F., Lin, L., Timmermann, A., & Zhao, J. (2007). Ensemble-mean dynamics of the ENSO recharge oscillator under state-dependent stochastic forcing. *Geophysical Research Letters*, *34*(3), L03807. https://doi.org/10.1029/2006GL027372

Kang, I.-S., & Kug, J.-S (2002). El Niño and La Niña sea surface temperature anomalies: Asymmetry characteristics associated with their wind stress anomalies. *Journal of Geophysical Research: Atmospheres, 107,* 1-10. https://doi.org/10.1029/2001JD000393

Kessler, W. S. (2002). Is ENSO a cycle or a series of events?. Geophysical Research Letters, 29(23), 40-1.

Kessler, W. S., McPhaden, M. J., & Weickmann, K. M. (1995). Forcing of intraseasonal Kelvin waves in the equatorial Pacific. *Journal of Geophysical Research*, *100*(C6), 10613–10631. https://doi.org/10.1029/95JC00382

Kim ST, Jin FF (2011) An ENSO stability analysis. Part II: results from the twentieth and twenty-first century simulations of the CMIP3 models. Clim Dyn 36:1609.

Kim, G.-I., and J.-S. Kug (2020), Tropical Pacific decadal variability induced by nonlinear rectification of El Nino-Southern Oscillation. J. Climate. 33:7289-7302.

Kim, S-K, and S-I. An, 2020: Untangling El Nino-La Nina asymmetries using a nonlinear coupled dynamics index. Geophy. Res. Lett., e2019GL085881. https://doi.org/10.1029/2019GL085881.

Kim, S.-K., & An, S.-I. (2021). Seasonal Gap Theory for ENSO Phase Locking, *Journal of Climate*, *34*(14), 5621-5634. https://doi.org/10.1175/jcli-d-20-0495.1

Kleeman, R. (2008). Stochastic theories for the irregularity of ENSO. *Philosophical Transactions of the Royal Society A: Mathematical, Physical and Engineering Sciences*, *366*(1875), 2509-2524.

Knutson, T. R. & Manabe, S. (1995): Time-Mean Response over the Tropical Pacific to Increased C02 in a Coupled Ocean-Atmosphere Model. J. Clim. 8, 2181–2199.

Kug JS, Li T, An S Il, et al (2006) Role of the ENSO-Indian Ocean coupling on ENSO variability in a coupled GCM. Geophys Res Lett 33: L09710.

Kug, J. S., Vialard, J., Ham, Y. G., Yu, J. Y., & Lengaigne, M. (2020). ENSO Remote forcing: influence of climate variability outside the tropical Pacific. *El Niño Southern Oscillation in a Changing Climate*, 247-265.

Kug, J.-S., Jin, F.-F., Sooraj, K. P., & Kang, I.-S. (2008). State-dependent atmospheric noise associated with ENSO. *Geophysical Research Letters, 35,* L05701. doi:10.1029/2007GL032017

Kug, J. S., Jin, F. F., & An, S. I. (2009). Two types of El Niño events: cold tongue El Niño and warm pool El Niño. Journal of climate, 22(6), 1499-1515.

Lee, S., L'Heureux, M., Wittenberg, A.T. et al. On the future zonal contrasts of equatorial Pacific climate: Perspectives from Observations, Simulations, and Theories. npj Clim Atmos Sci 5, 82 (2022). https://doi.org/10.1038/s41612-022-00301-2.

Lengaigne, M., Boulanger, J. P., Menkes, C., Delecluse, P., & Slingo, J. (2004a). Westerly wind events in the tropical Pacific and their influence on the coupled ocean-atmosphere system. *Earth Climate: The Ocean-Atmosphere Interaction, Geophys. Monogr*, *147*, 49-69.

Levine, A. F. Z., & Jin, F.-F. (2010). Noise-induced instability in the ENSO recharge oscillator. *Journal of the Atmospheric Sciences*, *67*(2), 529–542. https://doi.org/10.1175/2009JAS3213.1

Levine, A. F., & Jin, F. F. (2017). A simple approach to quantifying the noise–ENSO interaction. Part I: Deducing the state-dependency of the windstress forcing using monthly mean data. *Climate Dynamics*, *48*, 1-18.

Levine, A. F., & McPhaden, M. J. (2015). The annual cycle in ENSO growth rate as a cause of the spring predictability barrier. Geophysical Research Letters, 42(12), 5034-5041.

Levine, A.F.Z., F.F. Jin, M.J. McPhaden, 2016: Extreme Noise-Extreme El Niño: How State-Dependent Noise Forcing Creates El Niño-La Niña Asymmetry. J. Climate, 29, 5483-5499. DOI: http://dx.doi.org/10.1175/JCLI-D-16-0091.1

Lian, T., Chen, D., Tang, Y., Liu, X., Feng, J., & Zhou, L. (2018). Linkage between westerly wind bursts and tropical cyclones. Geophysical Research Letters, 45, 11,431–11,438. https://doi.org/10.1029/2018GL079745

Liu, Z., and B. Huang, 1997: A coupled theory of tropical climatology: Warm pool, cold tongue, and Walker circulation. J. Climate, 10, 1662–1679.

Liu, F., Vialard, J., Fedorov, A. V., Éthé, C., Person, R., Zhang, W., & Lengaigne, M. (2024). Why do oceanic nonlinearities contribute only weakly to extreme El Niño events? Geophysical Research Letters, 51, e2024GL108813. https://doi.org/10.1029/2024GL108813

Lopez, H, S.-K. Lee, D. Kim, A. T. Wittenberg, and S.-W. Yeh, 2022: Projections of faster onset and slower decay of El Niño in the 21st century. Nature Communications, 13, 1915. https://doi.org/10.1038/s41467-022-29519-7

Lu, B., Jin, F. F., & Ren, H. L. (2018). A coupled dynamic index for ENSO periodicity. *Journal of Climate*, *31*(6), 2361-2376.

Luo JJ, Wang G, Dommenget D (2018) May common model biases reduce CMIP5's ability to simulate the recent Pacific La Niña- like cooling? Clim Dyn 50:1335–1351. https://doi.org/10.1007/ s00382-017-3688-8.

Maher, N., Wills, R. C. J., DiNezio, P., Klavans, J., Milinski, S., Sanchez, S. C., ... & Wu, X. (2022). The future of the El Niño-Southern Oscillation: Using large ensembles to illuminate time-varying responses and inter-model differences. *Earth System Dynamics Discussions*, *2022*, 1-28.

McGregor, S., Timmermann, A., Schneider, N., Stuecker, M. F., & England, M. H. (2012). The Effect of the South Pacific Convergence Zone on the Termination of El Niño Events and the Meridional Asymmetry of ENSO, Journal of Climate, 25(16), 5566-5586. https://doi.org/10.1175/JCLI-D-11-00332.1

McGregor, S., Timmermann, A., Stuecker, M. et al. Recent Walker circulation strengthening and Pacific cooling amplified by Atlantic warming. Nature Clim Change 4, 888–892 (2014). https://doi.org/10.1038/nclimate2330.

McGregor S, Stuecker MF, Kajtar JB, England MH, Collins M (2018) Model tropical Atlantic biases underpin diminished Pacific decadal variability. Nat Clim Change 8:493–498. https://doi. org/ 10. 1038/ s41558-018- 0163-4

McGregor, S., Dommenget, D., & Neske, S. (2022). Distinct off-equatorial zonal wind stress and oceanic responses for EP-and CP-type ENSO events. Journal of Climate, 35(5), 1423-1440.

McPhaden, M. J., Lee, T., Fournier, S., & Balmaseda, M. A. (2020a). ENSO observations. *El Niño Southern Oscillation in a Changing Climate*, 39-63.

McPhaden, M.J., A. Santoso, and W. Cai, 2020b: Introduction to El Niño Southern Oscillation in a Changing Climate. In El Niño Southern Oscillation in a Changing Climate (eds M.J. McPhaden, A. Santoso and W. Cai). AGU Monograph, doi:10.1002/9781119548164.ch1.

McPhaden, M. J., 2015: Playing hide and seek with El Niño. Nature Climate Change, 5, 791-795.

McPhaden, M. J., Zebiak, S. E., & Glantz, M. H. (2006). ENSO as an integrating concept in earth science. science, 314(5806), 1740-1745.

McPhaden, M.J., 2003: Tropical Pacific Ocean heat content variations and ENSO persistence barriers. Geophys. Res. Lett., 30(9), 1480, doi:10.1029/2003GL016872.

Meinen, C. S., & McPhaden, M. J. (2000). Observations of warm water volume changes in the equatorial Pacific and their relationship to El Niño and La Niña. *Journal of Climate*, *13*(20), 3551-3559.

Neske, S., and S.McGregor, S., 2018: Understanding the warm water volume precursor of ENSO events and its interdecadal variation. Geophysical Research Letters, 45, 1577–1585. https:// doi.org/10.1002/2017GL076439

Ohba, M., & Ueda, H. (2007). An Impact of SST Anomalies in the Indian Ocean in Acceleration of the El Niño to La Niña Transition. *Journal of the Meteorological Society of Japan, 85,* 335–348. https://doi.org/10.2151/jmsj.85.335

Okumura, Y. M., & Deser, C. (2010). Asymmetry in the duration of El Niño and La Niña. *Journal of Climate, 23,* 5826–5843. https://doi.org/10.1175/2010JCLI3592.1

Philander, S.G. and Fedorov, A., 2003. Is El Niño sporadic or cyclic?. Annual Review of Earth and Planetary Sciences, 31(1), pp.579-594.

Picaut, J., F. Masia, and Y. du Penhoat (1997). An advective-reflective conceptual model for the oscillatory nature of the ENSO. *Science*, 277, 663-666.

Planton, Y. Y., Guilyardi, E., Wittenberg, A. T., Lee, J., Gleckler, P. J., Bayr, T., McGregor, S., McPhaden, M. J., Power, S., Roehrig, R., Vialard, J., & Voldoire, A. (2021). Evaluating Climate Models with the CLIVAR 2020 ENSO Metrics Package, *Bulletin of the American Meteorological Society*, *102*(2), E193-E217. https://doi.org/10.1175/BAMS-D-19-0337.1

Planton, Y. Y., Vialard, J., Guilyardi, E., Lengaigne, M., & Mcphaden, M. J. (2021). The asymmetric influence of ocean heat content on ENSO predictability in the CNRM-CM5 coupled general circulation model. *Journal of Climate*, *34*(14), 5775-5793.

Planton, Y., Vialard, J., Guilyardi, E., Lengaigne, M., & Izumo, T. (2018). Western Pacific oceanic heat content: A better predictor of La Niña than of El Niño. *Geophysical Research Letters*, *45*(18), 9824-9833.

Power, S., Lengaigne, M., Capotondi, A., Khodri, M., Vialard, J., Jebri, B., ... & Henley, B. J. (2021). Decadal climate variability in the tropical Pacific: Characteristics, causes, predictability, and prospects. *Science*, *374*(6563).

Praveen Kumar, B., J. Vialard, M. Lengaigne, V. S. N. Murty, and M. J. McPhaden, 2012: TropFlux: Air–sea fluxes for the global tropical oceans—Description and evaluation. Climate Dyn., 38, 1521–1543, https://doi.org/10.1007/s00382-011-1115-0.

Praveen Kumar, B., J. Vialard, M. Lengaigne, V. S. N. Murty, M. J. McPhaden, M. F. Cronin, F. Pinsard, and K. Gopala Reddy, 2013: TropFlux wind stresses over the tropical oceans: Evaluation and comparison with other products. Climate Dyn., 40, 2049–2071, https://doi.org/10.1007/s00382-012-1455-4.

Puy, M., Vialard, J., Lengaigne, M., & Guilyardi, E. (2016). Modulation of equatorial Pacific westerly/easterly wind events by the Madden–Julian oscillation and convectively-coupled Rossby waves. *Climate dynamics*, *46*, 2155-2178.

Puy, M., Vialard, J., Lengaigne, M., Guilyardi, E., DiNezio, P. N., Voldoire, A., ... & Mcphaden, M. J. (2019). Influence of westerly wind events stochasticity on El Niño amplitude: The case of 2014 vs. 2015. *Climate Dynamics*, *52*, 7435-7454.

Rayner, N. A.; Parker, D. E.; Horton, E. B.; Folland, C. K.; Alexander, L. V.; Rowell, D. P.; Kent, E. C.; Kaplan, A. (2003) Global analyses of sea surface temperature, sea ice, and night marine air temperature since the late nineteenth century J. Geophys. Res.Vol. 108, No. D14, 4407 10.1029/2002JD002670

Rio, M. H., Mulet, S., & Picot, N. (2014). Beyond GOCE for the ocean circulation estimate: Synergetic use of altimetry, gravimetry, and in situ data provides new insight into geostrophic and Ekman currents. *Geophysical Research Letters*, *41*(24), 8918-8925.

Seager, R., Henderson, N. & Cane, M. Persistent Discrepancies between Observed and Modeled Trends in the Tropical Pacific Ocean. J. Clim. 35, 4571–4584 (2022).

Shin, NY., Kug, JS., Stuecker, M.F. et al. More frequent central Pacific El Niño and stronger eastern pacific El Niño in a warmer climate. npj Clim Atmos Sci 5, 101 (2022). https://doi.org/10.1038/s41612-022-00324-9.

Srinivas, G., Vialard, J., Liu, F., Voldoire, A., Izumo, T., Guilyardi, E., & Lengaigne, M. (2024). Dominant contribution of atmospheric nonlinearities to ENSO asymmetry and extreme El Niño events. *Scientific Reports*, *14*(1), 8122.

Stein, K., Schneider, N., Timmermann, A., & Jin, F. F. (2010). Seasonal synchronization of ENSO events in a linear stochastic model. *Journal of Climate*, *23*(21), 5629–5643. https://doi.org/10.1175/2010JCLI3292.1

Stein, K., Timmermann, A., Schneider, N., Jin, F. F., & Stuecker, M. F. (2014). ENSO seasonal synchronization theory. *Journal of Climate*, *27*(14), 5285–5310. https://doi.org/10.1175/JCLI-D-13-00525.1

Stuecker, M. F., Timmermann, A., Jin, F. F., McGregor, S., & Ren, H. L. (2013). A combination mode of the annual cycle and the El Niño/Southern Oscillation. *Nature Geoscience*, *6*(7), 540–544. https://doi.org/10.1038/ngeo1826

Stuecker, M. F., Timmermann, A., Jin, F.-F., Chikamoto, Y., Zhang, W., Wittenberg, A. T., Widiasih, E., and Zhao, S. (2017), Revisiting ENSO/Indian Ocean Dipole phase relationships, Geophys. Res. Lett., 44, 2481–2492, doi:10.1002/2016GL072308.

Stuecker, M.F. Revisiting the Pacific Meridional Mode. Sci Rep 8, 3216 (2018). https://doi.org/10.1038/s41598-018-21537-0

Stuecker, M.F. The climate variability trio: stochastic fluctuations, El Niño, and the seasonal cycle. *Geosci. Lett.* **10**, 51 (2023). https://doi.org/10.1186/s40562-023-00305-7

Suarez, M. J., and P. S. Schopf (1988). A delayed action oscillator for ENSO. *J. Atmos. Sci*., 45, 3283-3287.

Sun, De-Zheng, and Zhengyu Liu. 1996. 'Dynamic Ocean-Atmosphere Coupling: A Thermostat for the Tropics'. Science 272 (5265): 1148–50.

Takahashi, K., A. Montecinos, K. Goubanova, and B. Dewitte (2011), ENSO regimes: Reinterpreting the canonical and Modoki El Niño, Geophys. Res. Lett., 38, L10704,doi:10.1029/2011GL047364.

Takahashi, K., Karamperidou, C., & Dewitte, B. (2019). A theoretical model of strong and moderate El Niño regimes. *Climate Dynamics*, *52*(12), 7477–7493. https://doi.org/10.1007/s00382-018-4100-z

Taschetto, A. S., Ummenhofer, C. C., Stuecker, M. F., Dommenget, D., Ashok, K., Rodrigues, R. R., & Yeh, S. W. (2020). ENSO atmospheric teleconnections. *El Niño southern oscillation in a changing climate*, 309-335.

Thual, S., Dewitte, B., An, S.-I. & Ayoub, N. Sensitivity of ENSO to stratification in a recharge–discharge conceptual model. J. Clim. 4, 4331–4348 (2011).

Thual, S., & Dewitte, B. (2023). ENSO complexity controlled by zonal shifts in the Walker circulation. Nature Geoscience, 16(4), 328-332.

Timmermann, A., Jin, F.-F., & Abshagen, J. (2003). A nonlinear theory for El Niño Bursting. Journal of the Atmospheric Sciences, 60(1), 152–165. https://doi.org/10.1175/1520-0469(2003)060<0152:antfen>2.0.co;2

Timmermann, A., An, S. I., Kug, J. S., Jin, F. F., Cai, W., Capotondi, A., ... & Zhang, X. (2018). El Niño–southern oscillation complexity. Nature, 559(7715), 535-545.

Trenberth, K. E. (2020). ENSO in the global climate system. *El Niño Southern Oscillation in a Changing Climate*, 21-37.

Tziperman, E., Cane, M. A., & Zebiak, S. E. (1995). Irregularity and locking to the seasonal cycle in an ENSO prediction model as explained by the quasi-periodicity route to chaos. Journal of Atmospheric Sciences, 52(3), 293-306.

Vecchi, Gabriel A., Brian J. Soden, Andrew T. Wittenberg, Isaac M. Held, Ants Leetmaa, and Matthew J. Harrison. 2006. 'Weakening of Tropical Pacific Atmospheric Circulation Due to Anthropogenic Forcing'. Nature 441 (7089): 73–76.

Vialard, J., Menkes, C., Boulanger, J. P., Delecluse, P., Guilyardi, E., McPhaden, M. J., & Madec, G. (2001). A model study of oceanic mechanisms affecting equatorial Pacific sea surface temperature during the 1997–98 El Niño. *Journal of Physical Oceanography*, *31*(7), 1649-1675.

Vijayeta, A., & Dommenget, D. (2018). An evaluation of ENSO dynamics in CMIP simulations in the framework of the recharge oscillator model. *Climate Dynamics*, *51*(5), 1753-1771.

Vimont, D, Battisti, D, and Hirst, A. Footprinting: A Seasonal Connection Between the Tropics and Mid-Latitudes. *Geophys Res Lett* 2001; **28**: 3923-3926.

Wang, C. (2001). A unified oscillator model for the El Niño-Southern Oscillation. *J. Clim*., 14, 98-115.

Wang, C. (2018). A review of ENSO theories. *National Science Review*, 5, 813–825.

Wang, C., & Picaut, J. (2004). Understanding ENSO physics—A review. *Earth's Climate: The Ocean–Atmosphere Interaction, Geophys. Monogr*, *147*, 21-48.

Wang, C., R. H. Weisberg, and J. I. Virmani (1999). Western Pacific interannual variability associated with the El Niño-Southern Oscillation. *J. Geophys. Res*., 104, 5131-5149.

Wang, W. and M.J. McPhaden, 2000: The surface layer heat balance in the equatorial Pacific Ocean. Part II: Interannual variability. J. Phys. Oceanogr., 30, 2989–3008.

Watanabe M, Jin F (2002) Role of Indian Ocean warming in the development of Philippine Sea anticyclone during ENSO. Geophys Res Lett 29:116–1–116–4.

Watanabe, M., Kang, S. M., Collins, M., Hwang, Y. T., McGregor, S., & Stuecker, M. F. (2024). Possible shift in controls of the tropical Pacific surface warming pattern. Nature, 630(8016), 315-324.

Weisberg, R. H., and C. Wang (1997). A western Pacific oscillator paradigm for the El Niño-Southern Oscillation. *Geophys. Res. Lett*., 24, 779-782.

Wengel, C., Lee, SS., Stuecker, M.F. et al. Future high-resolution El Niño/Southern Oscillation dynamics. Nat. Clim. Chang. 11, 758–765 (2021).

Willett, C. S., Leben, R. R., & Lavín, M. F. (2006). Eddies and tropical instability waves in the eastern tropical Pacific: A review. *Progress in Oceanography*, *69*(2-4), 218-238.

Wills, R. C. J., Dong, Y., Proistosecu, C., Armour, K. C., & Battisti, D. S. (2022). Systematic climate model biases in the large-scale patterns of recent sea-surface temperature and sea-level pressure change. Geophysical Research Letters, 49, e2022GL100011. https://doi. org/10.1029/2022GL100011.

Wittenberg, A. T., 2009: Are historical records sufficient to constrain ENSO simulations? Geophys. Res. Lett., 36, L12702. https://doi.org/10.1029/2009GL038710

Wittenberg, A. T., A. Rosati, T. L. Delworth, G. A. Vecchi, and F. Zeng, 2014: ENSO modulation: Is it decadally predictable? J. Climate, 27, 2667-2681. https://doi.org/10.1175/JCLI-D-13-00577.1

Wyrtki, K. (1985). Water displacements in the Pacific and the genesis of El Niño cycles. *Journal of Geophysical Research: Oceans*, *90*(C4), 7129-7132.

Xie SP, Hu K, Hafner J, et al (2009) Indian Ocean capacitor effect on Indo-Western pacific climate during the summer following El Niño. J Clim 22:730–747.

Xie, S.P., Deser, C., Vecchi, G.A., Ma, J., Teng, H. and Wittenberg, A.T., 2010. Global warming pattern formation: Sea surface temperature and rainfall. Journal of Climate, 23(4), pp.966-986.

Yu, J.-Y., C. R. Mechoso, J. C. McWilliams, and A. Arakawa (2002), Impacts of the Indian Ocean on the ENSO cycle, Geophys. Res. Lett., 29(8), 1204, doi:10.1029/2001GL014098.

Yu, S. and Fedorov, A.V., 2022: The essential role of westerly wind bursts in shaping ENSO characteristics and extreme events in model "wind stress shaving" experiments. *Journal of Climate*, 1-62.

Zhang, L., & Li, T. (2014). A Simple Analytical Model for Understanding the Formation of Sea Surface Temperature Patterns under Global Warming. Journal of Climate, 27(22), 8413–8421. https://doi.org/10.1175/jcli-d-14-00346.1

Zhang, W., Jiang, F., Stuecker, M.F. et al. Spurious North Tropical Atlantic precursors to El Niño. Nat Commun 12, 3096 (2021). https://doi.org/10.1038/s41467-021-23411-6

Zhao, B. and Fedorov, A., 2020: The effects of background zonal and meridional winds on ENSO in a coupled GCM. *Journal of Climate*, *33*, 2075-2091.

Zhao, S., Jin, F.-F., & Stuecker, M. F. (2021). Understanding Lead Times of Warm Water Volumes to ENSO Sea Surface Temperature Anomalies. Geophysical Research Letters, 48(19), e2021GL094366. https://doi.org/10.1029/2021GL094366.

Zhao, S., Jin, F. F., Stuecker, M. F., Thompson, P. R., Kug, J. S., McPhaden, M. J., ... & Cai, W. (2024). Explainable El Niño predictability from climate mode interactions. Nature, 630(8018), 891-898.

Zuo, H., Balmaseda, M. A., Tietsche, S., Mogensen, K., & Mayer, M. (2019). The ECMWF operational ensemble reanalysis–analysis system for ocean and sea ice: a description of the system and assessment. *Ocean science*, *15*(3), 779-808.

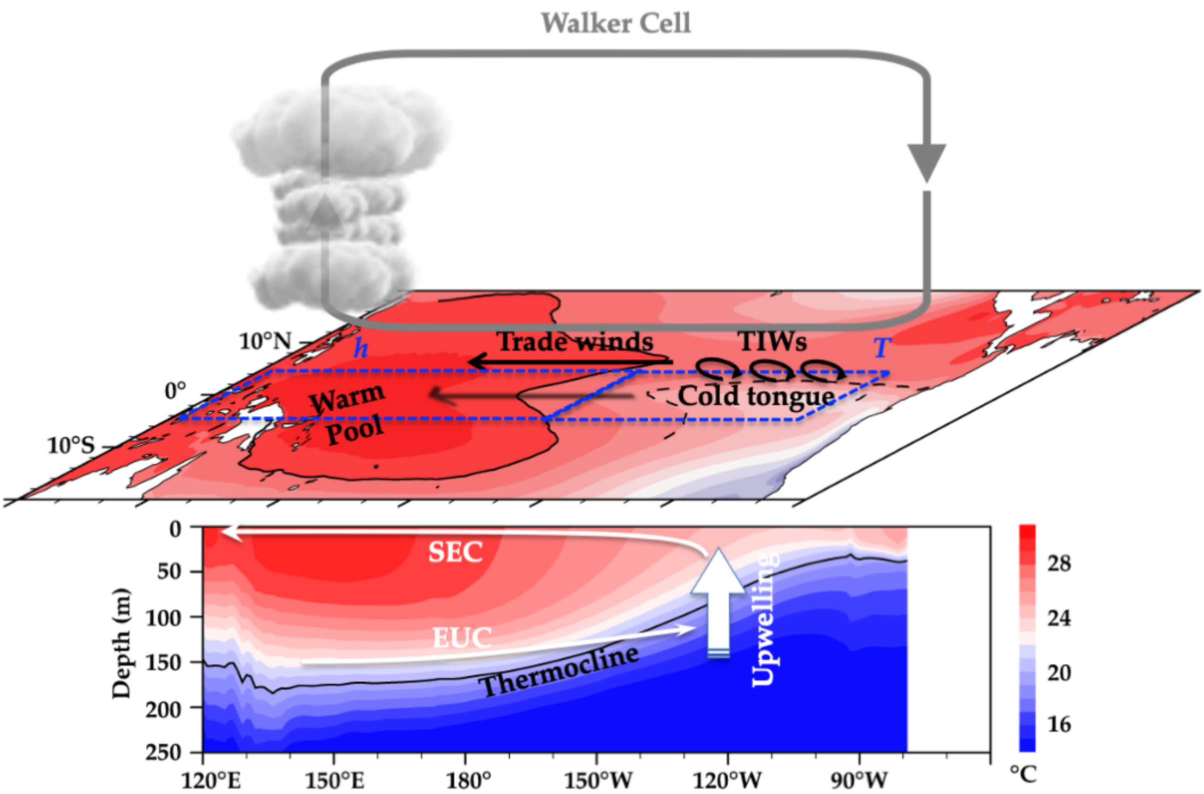

Figure 1. The tropical Pacific mean state. Sketch of the equatorial Pacific "normal" state, over which anomalies associated with ENSO develop. The shading indicates the climatological Sea Surface Temperature (SST) and temperature vertical structure along the equator (ORAS5 data, 1958-2020 September-November average). Trade winds are the surface branch of the equatorial plane atmospheric circulation cell known as the Walker cell, and energized by SST contrasts between the eastern Pacific (cold tongue) and western Pacific (Warm pool). The easterly trade winds in return drive upwelling and the cold tongue in the east. The positive feedback loop between the equatorial SST and trade winds is known as the Bjerknes feedback. The dashed lines delineate the western Pacific (5°N-5°S, 120°W-150°W) and Niño3 (5°N-5°S, 150°W-90°W) averaging regions that are usually used for defining the equatorial Pacific heat content h and surface temperature T variables used in the recharge oscillator, although some other choices (such as the average heat content in the entire equatorial Pacific or the 5°N-5°S, 170°W-120°W Niño3.4 region) are sometimes made. The approximate locations for the western Pacific Warm Pool, Eastern equatorial Pacific Cold Tongue and upwelling, region where Tropical Instability Waves (TIWs) occur, thermocline (here the 20°C isotherm), South Equatorial Current (SEC) and Equatorial Undercurrent (EUC) are marked on the Figure. See section 2.1 for more details on the other elements on this figure.

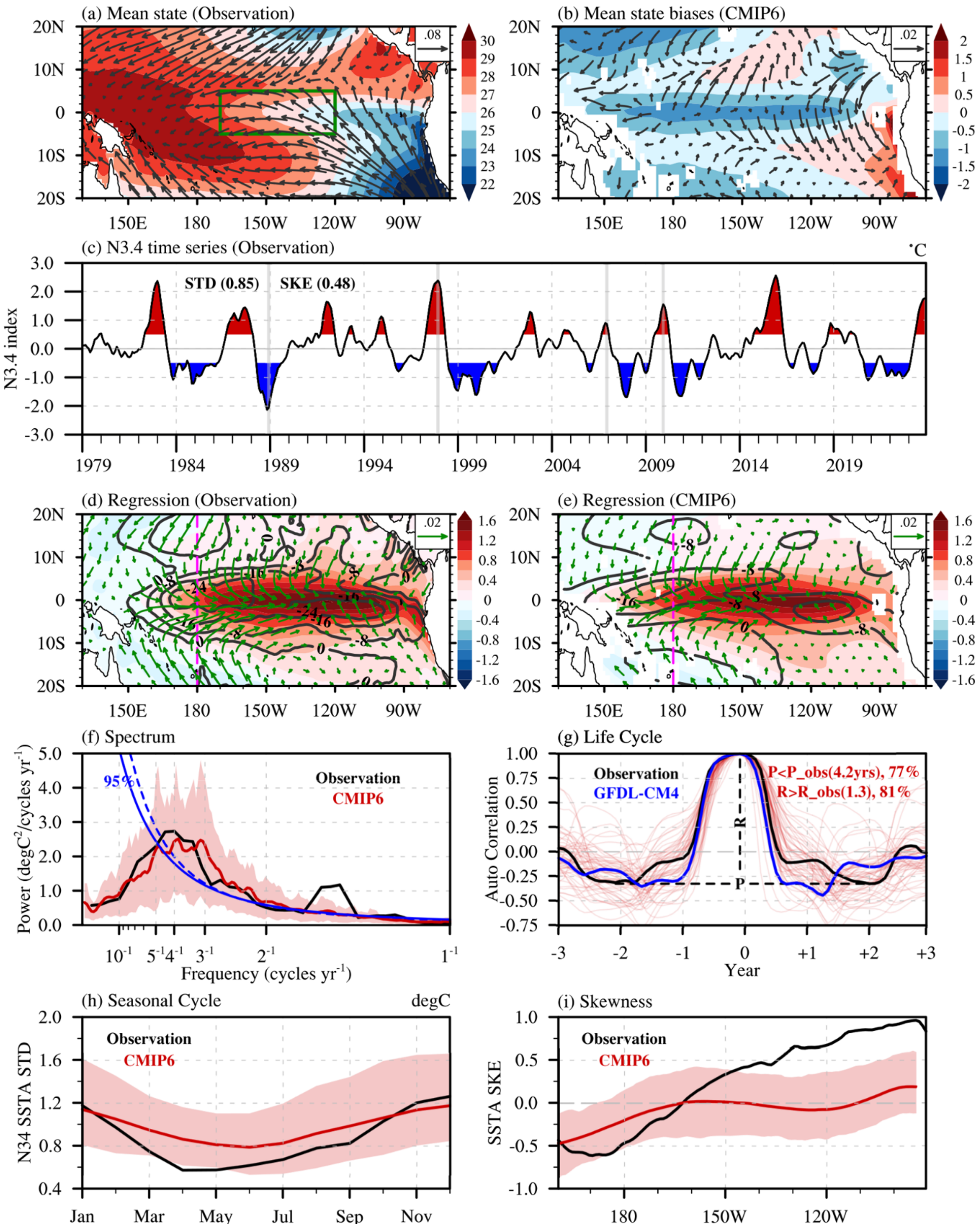

***Figure 2. ENSO properties in observations and climate models*. (a)** Observed SST (shading, °C) and wind stress (vectors, Nm^{-2}) tropical Pacific long-term climatology (1979-2023, HadiSST). **(b)** Multi model-mean from 57 CMIP6 historical runs minus (a). **(c)** Times series of observed average Niño-3.4 SST anomalies during 1979-2018. **(d)** Typical ENSO SST (shading, °C), wind stress (vectors, Nm^{-2}) and net heat flux (contours , only negative values, Wm^{-2}) observed spatial pattern (obtained by regressing average November-January (NDJ) anomalies on the normalized NDJ Niño-3.4 index). **(e)** As (d), but for the CMIP6 models ensemble mean.

(f) Spectrum of the Niño-3.4 indices for observation (black) and CMIP6 models (red with the line indicating the ensemble mean). The dashed and solid blue curves indicate 95% confidence level for observation and CMIP6 models, respectively. **(g)** ENSO life cycle for observation (black) and CMIP6 models (light red, 1 curve per model), obtained from the lagged auto-correlation of NDJ Niño-3.4 index. The dashed lines indicate how the periodicity (P) and regularity (R) metrics are defined for observations following Jiang et al. 2021. P is the time lag of the maximum negative autocorrelation and R is1 minus the autocorrelation value at this lag. The GFDL-CM4 model (closest model to the median P and R values) is displayed as the blue curve. 81% of the CMIP6 models are more regular, and 77% have a shorter period than observations. **(h)** Seasonal cycle of Niño-3.4 SSTA standard deviation (°C) for observations (black) and CMIP6 models (red). **(i)** Skewness of 5°S-5°N averaged SST anomalies for observations (black) and CMIP6 models (red). The Niño-3.4 region is shown as a green box on (a). The pink lines in (d)-(f) indicate the dateline. The light red shadings in (f), (h) and (i) denote 10%-90% quartile range for CMIP6.

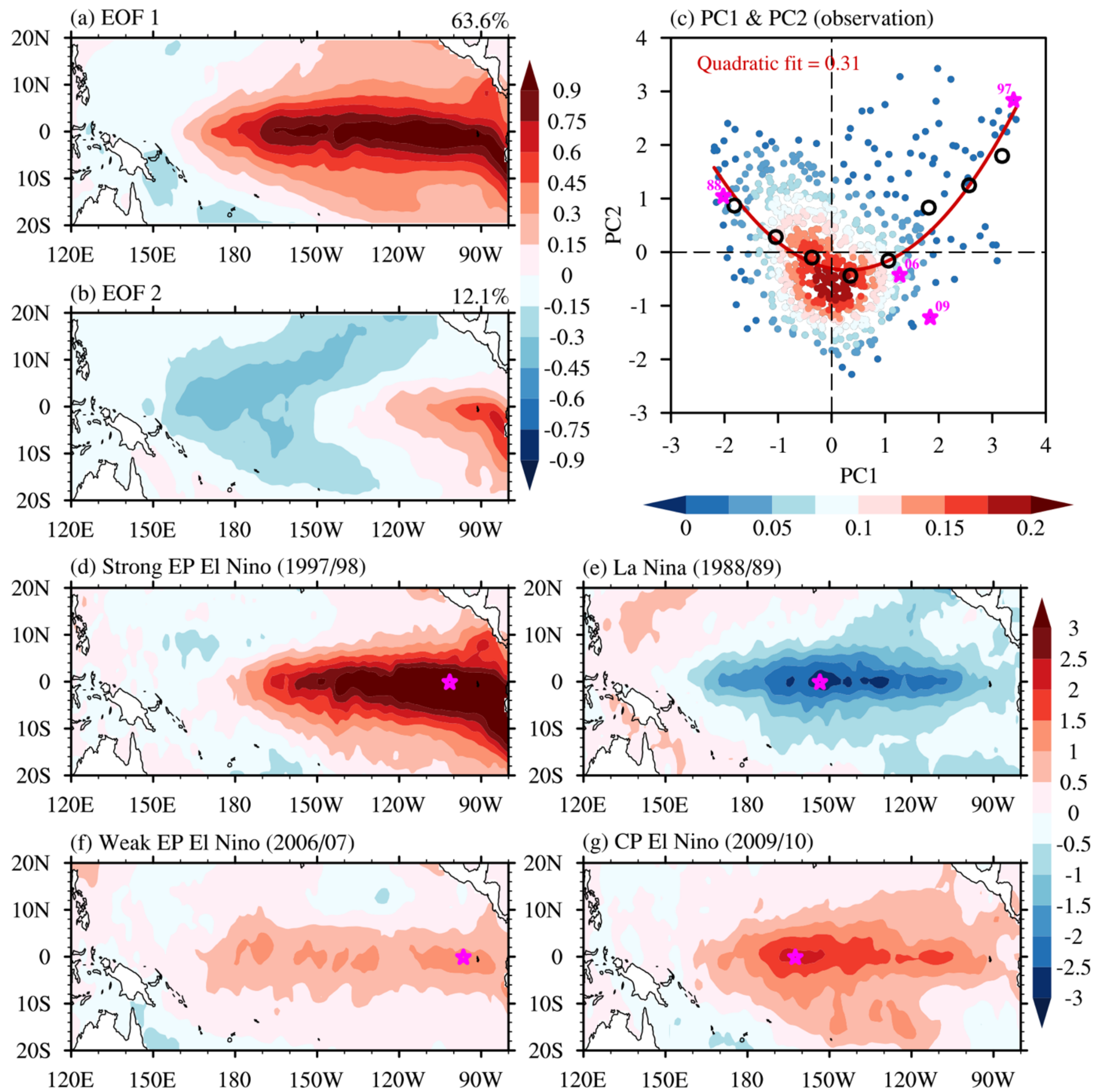

Figure 3. ENSO pattern diversity. **(a)** First and **(b)** second Empirical Orthogonal Functions (EOF) of the observed (HadISST, 1958-2020, 3-months sliding average) tropical Pacific SST anomalies. The principal component –PCs- have been normalized by their standard deviation so that the EOF is in physical units (°C). The percentage of the total variance explained by each EOF mode is indicated above panels a,b. (c-f) November to January averages of various years that illustrate the ENSO diversity: **(c)** 1997-98 strong EP El Niño, **(d)** 1998-89 La Niña, **(e)** 2006-07 weak EP El Niño and **(f)** 2009-10 weak CP El Niño event. **(g)** Scatterplot of the second versus the first normalized principal components (PC1 and PC2). A quadratic fit to the PC1,PC2 distribution is plotted in red, and the quadratic coefficient value is indicated on each panel. Purple stars on (c) indicate years for which the November-January maps of panels (c-f) were plotted. Purple stars on d-g indicate the longitude of the maximum 5°N-5°S average SST anomalies.

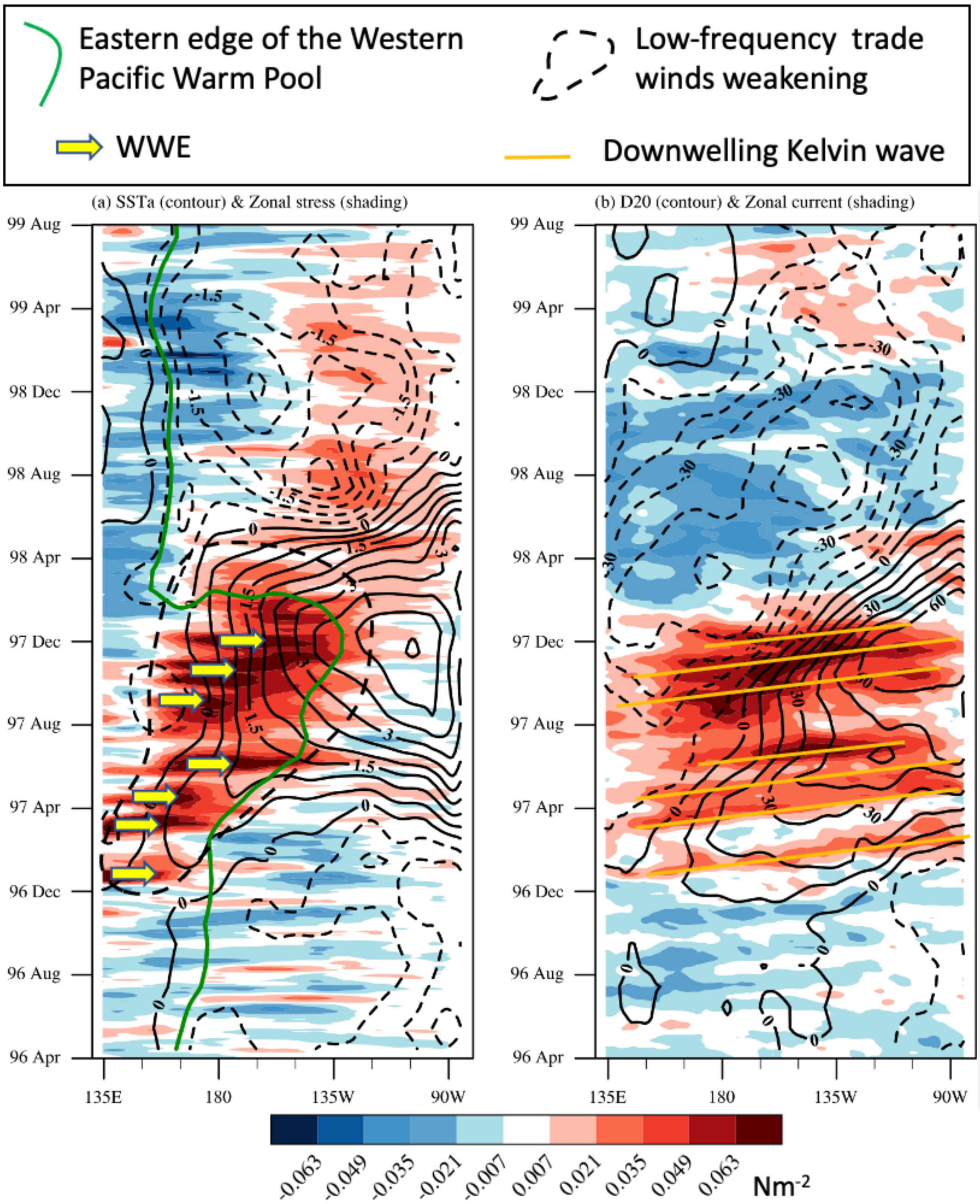

Figure 4. ENSO growth mechanisms, illustrated from the 1997-1998 strong El Niño. Time-longitude sections of 2°S–2°N average anomalous **(a)** SST (contours, °C) and zonal wind stress (shading, Nm^{-2}), **(b)** 20°C isotherm depth (D20), a proxy for the equatorial thermocline (contours, m) and 15m zonal current (shading, ms^{-1}) during the 1997-98 extreme El Niño event. We use monthly Tropflux SST, ORAS5 subsurface temperature, and daily zonal wind stress (TropFlux) and zonal currents (Globcurrent) anomalies relative to the 1993-2016 climatology. A 3-month (15-day) running filter is applied on SST and D20 (wind stress and current). A 10-degree running average is applied to all fields. The concurrent gradual weakening of the winds, deepening of the thermocline and SST warming during 1997 are manifestations of the Bjerknes feedback.

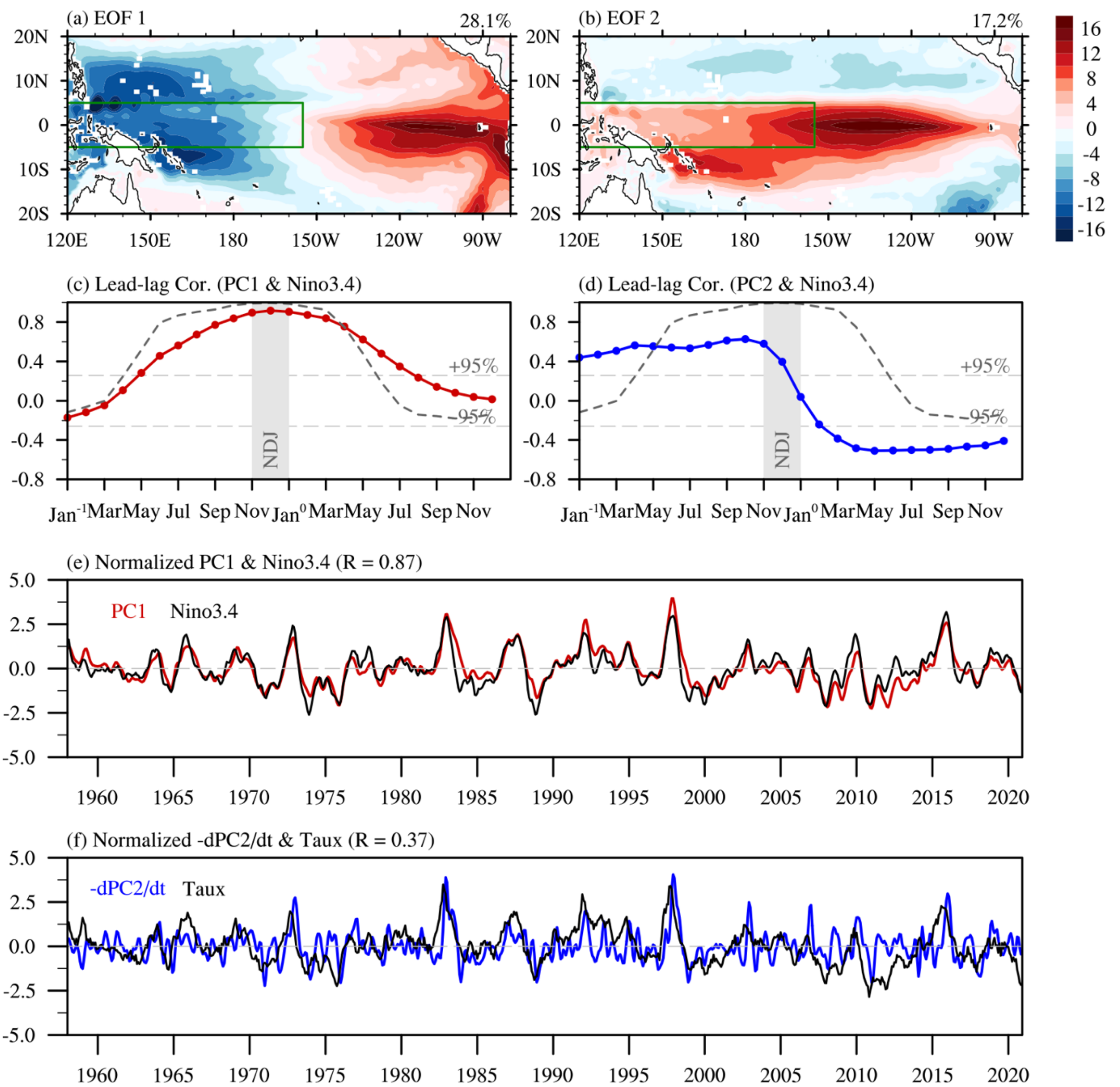

Figure 5. Equatorial heat content discharge/recharge. **(a)** First and **(b)** second EOF of the tropical Pacific ORAS5 D20 anomalies (m) over the 1958-2020 period, with % of explained total variance indicated at the top right. The green box delineates the western Pacific (5°N-5°S, 120°W-155°W) averaging region. **(c-d)** Lead-lag correlations between the winter (NDJ, grey shading) Niño-3.4 index and **(c)** the 1st EOF principal component (PC1, red dot curve) and **(d)** the 2nd EOF principal component (PC2, blue dot curve). The Niño-3.4 index lagged autocorrelation is indicated as a grey dashed curve on c, d. The light grey horizontal lines indicate the 95% confidence level. **(e)** Normalized PC1 (red) and Niño-3.4indices (black) time series. **(f)** Normalized –dPC2/dt (blue) and average central Pacific (150°E–130°W, 5°S–5°N) zonal wind stress anomalies (black). The correlation coefficients between the two curves on e and f are indicated on the panel title. A 3-month running average is applied to all the time series in (e) and (f).

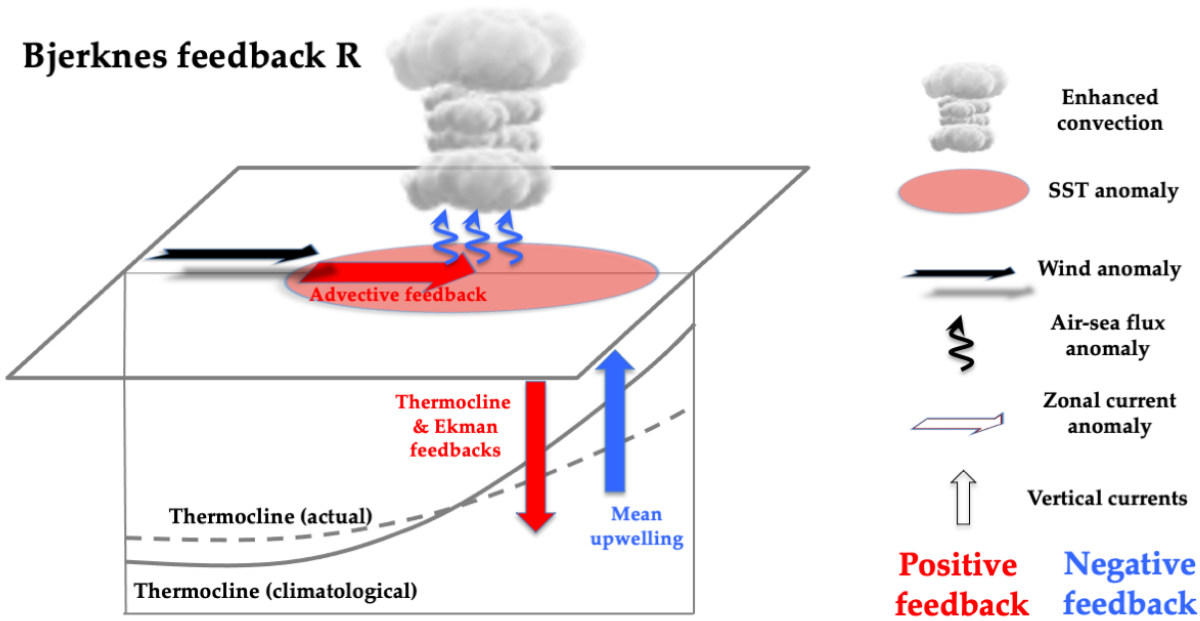

Figure 6*. *The Bjerknes feedback. Overview of the physical processes involved in the Bjerknes feedback loop, here for the example of a positive SST anomaly. A warm SST anomaly induces enhanced deep atmospheric convection, and westerly wind anomalies through the Gill (1980) response. This leads to negative surface heat flux anomalies (less shortwave, more evaporation), a negative feedback on the SST anomaly. The background circulation also tends to damp the warm anomaly, for instance through the mean upwelling of cold water. On the other hand, the fast oceanic response through downwelling Kelvin waves (assumed to be instantaneous in the RO) is associated with anomalous thermocline deepening in the eastern equatorial Pacific. The associated thermocline feedback favors the development of warm SST anomalies. Wind relaxation along the equator also contributes to surface warming through zonal, meridional and vertical (or Ekman) advection feedbacks. Together, these positive feedbacks control the strength of the Bjerknes feedback. The intensity of both positive and negative feedbacks depend on the background state, and the seasonal cycle leads to a slightly negative R value in spring and early summer. Positive feedbacks take over the thermal damping and damping by the mean circulation from roughly June to December (e.g. Jin, 2021). The overall ENSO stability given by $\frac{R-\varepsilon}{2}$ is usually positive in fall, and weakly negative on annual average (sections 4.1 and 4.2).

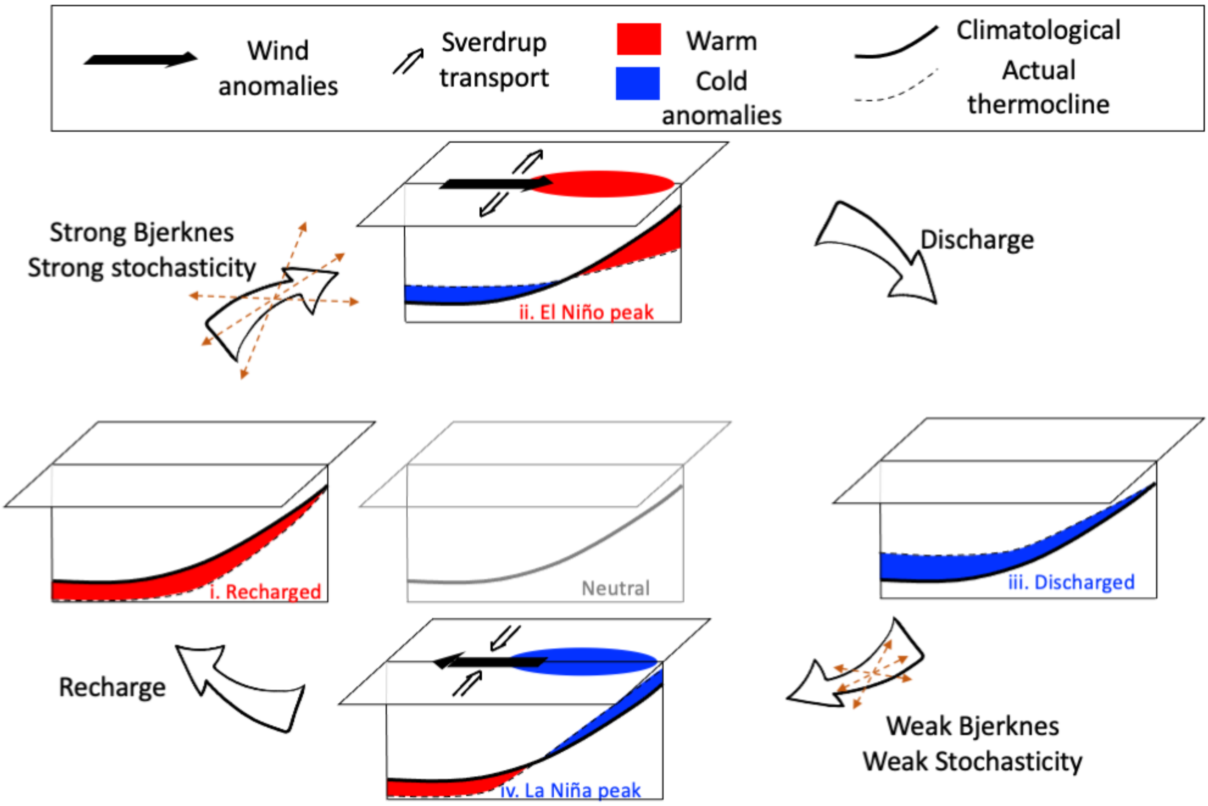

Figure 7. The RO mechanism for ENSO phase transitions. A recharged western Pacific heat content (i), favors the development of warm SST anomalies during summer and fall amplified by the Bjerknes feedback (see Fig. 6). Nonlinearities induce more WWBs stochasticity, leading to an uncertain evolution but also favoring the growth of positive T anomalies, possibly leading to stronger warm events than cold events. The westerly stress anomalies lead to a Sverdrup transport out of the equatorial band, inducing a discharge of the western Pacific heat content. The associated delayed advective and thermocline negative feedbacks end the El Niño event, and lead to a discharged state (iii). The transition to La Niña (iv) and to a recharged state (i) again occurs through symmetrical processes, but with less stochasticity due to weakly active WWBs, and symmetry breaking nonlinearity that favor smaller amplitude SST and recharge anomalies during and after La Niña. Stochasticity acts along the entire cycle, making it much more erratic than on this simplified sketch. For instance, stochasticity can represent a series of WWBs, which could lead to an El Niño, even in the absence of an initial positive heat content preconditioning. Stochasticity is enhanced when there are positive SST anomalies, making the evolution of El Niño less predictable than that of La Niña.

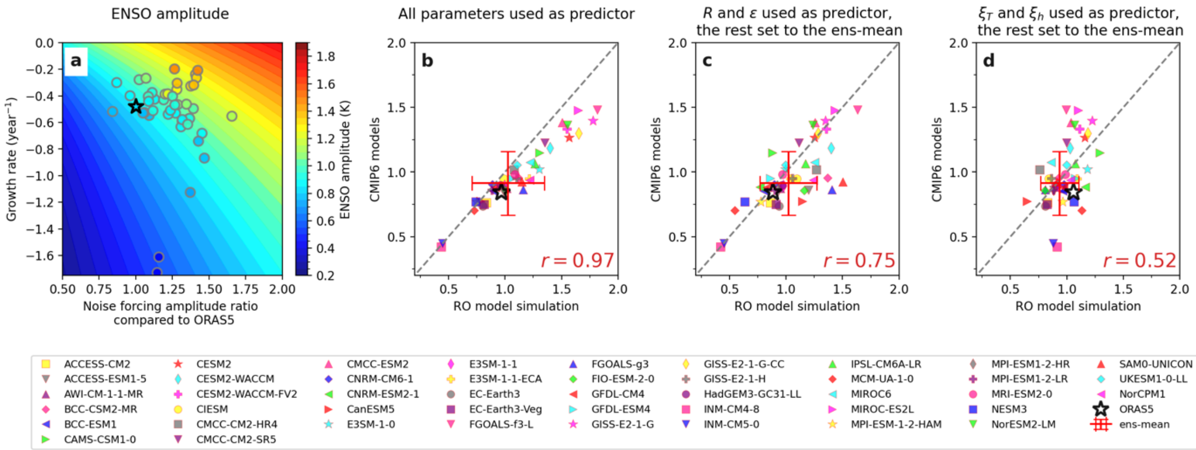

Figure 8: the RO reproduces ENSO amplitude. (**a**) ENSO amplitude in the NRO (details below), as a function of the growth rate $\frac{R-\varepsilon}{2}$ and noise forcing amplitude (ratio to that of ORAS5) (shading). Symbols indicate the fitted RO growth rate vs the noise forcing amplitude in 45 CMIP6 individual models (*circles*) and ORAS5 reanalysis (*pentagram*), with the color of the symbol indicating the ENSO amplitude . (**b-d**) Scatter plots of ENSO amplitude (K) in the CMIP6 models and ORAS5 (vertical axes) against that from the NRO simulation where (b) all NRO parameters are used, (c) only R and ε are used, (c) only ξ_T and ξ_h are used, with the other parameters set fixed at the ensemble-mean values. Using R, ε, ξ_T and ξ_h yields a 0.9 correlation with the actual ENSO amplitude (not shown). The CMIP6 ensemble-mean and one standard deviation spread is indicated by the red cross, and the linear correlation coefficient over all CMIP6 models is indicated in the lower right corner of each panel. The RO models used in the Figs. 8-12 original analyses are based on equations 4, 5, with h defined from the equatorial average heat content. The parameters were obtained from RO fit to observations or CMIP (see Table 2 for details and observed coefficient values). The stochastic forcing uses red noise for ξ_T; ξ_h, whose amplitude and ~1 month decorrelation are estimated based on residuals of the fit. Figure 8 is based on the nonlinear RO, with B and b set to zero (i.e. no *R(t)* seasonal dependency, c only non-zero nonlinear parameter as in Table 2).

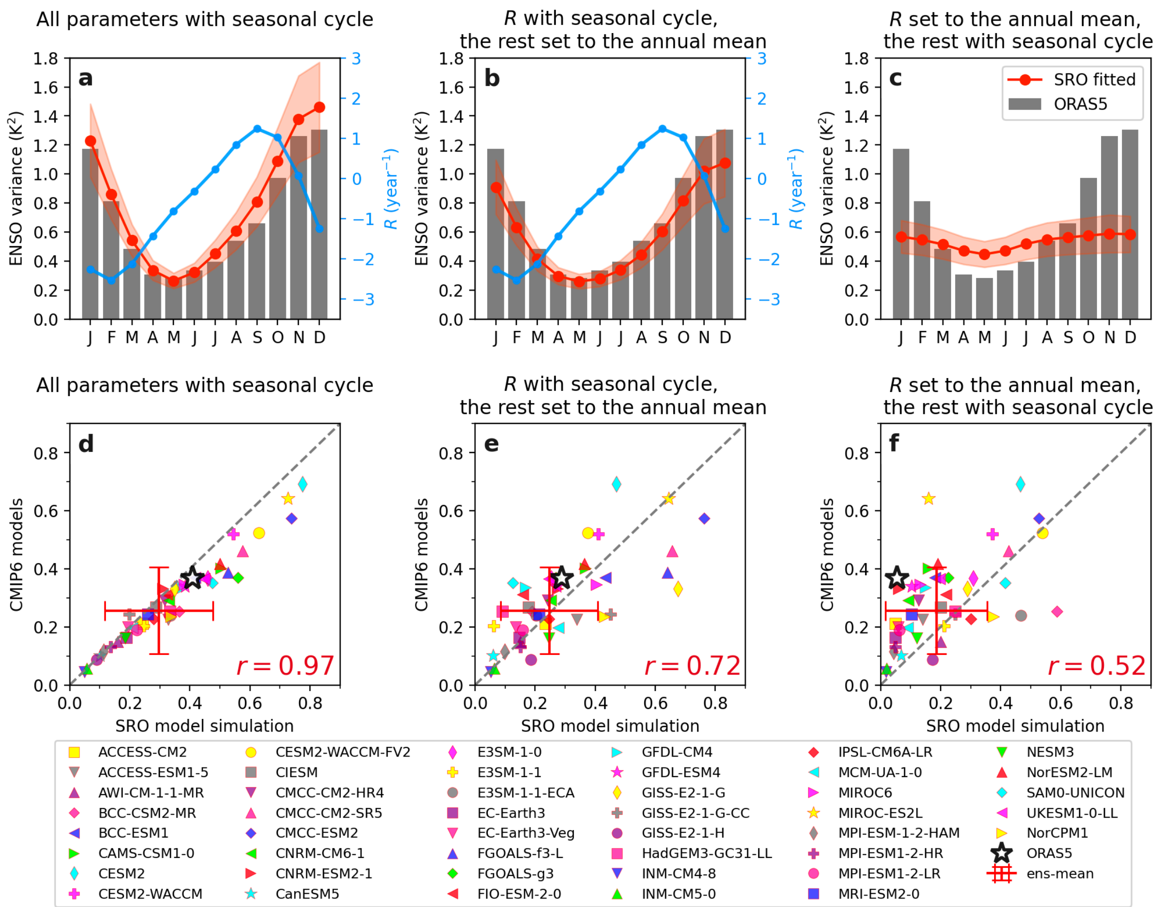

Figure 9: the RO reproduces ENSO seasonality. ENSO variance seasonal cycle in observation (bars) and that obtained from integrating the SRO model with parameters estimated for the observation (red curves): **(a)** all parameters with seasonal cycle, **(b)** only *R* with seasonal cycle and the other parameters set to the annual mean values, **(c)** *R* with annual mean, but other parameters with seasonal cycle. The seasonal cycle of *R* is displayed in blue on a-b. The shading indicates the one-standard deviation spread by splitting 3100-yrs simulations into 50 ensemble members with the same length of 62 yr with observation (1958-2020). **(d)** scatter plot of the amplitude of the seasonal cycle of ENSO standard deviation in CMIP6 against that obtained from integrating the NRO fitted to this model. **(e)** as (d) but with a seasonal cycle in R and other parameters set to their annual-mean values, **(f)** as (d) but with *R* set to its annual mean value and the full seasonal cycle for other parameters. The RO models used in the Figs. 8-12 original analyses are based on equations 4, 5, with *h* defined from the equatorial average heat content. The parameters were obtained from RO fit to observations or CMIP (see Table 2 for details and observed coefficient values). The stochastic forcing uses red noise for ξ_T; ξ_h, whose amplitude and ~1 month decorrelation are estimated based on residuals of the fit. Figure 9 uses the seasonally dependent stochastic RO (i.e. *R(t)* and *b*=*B*=*c*=0).

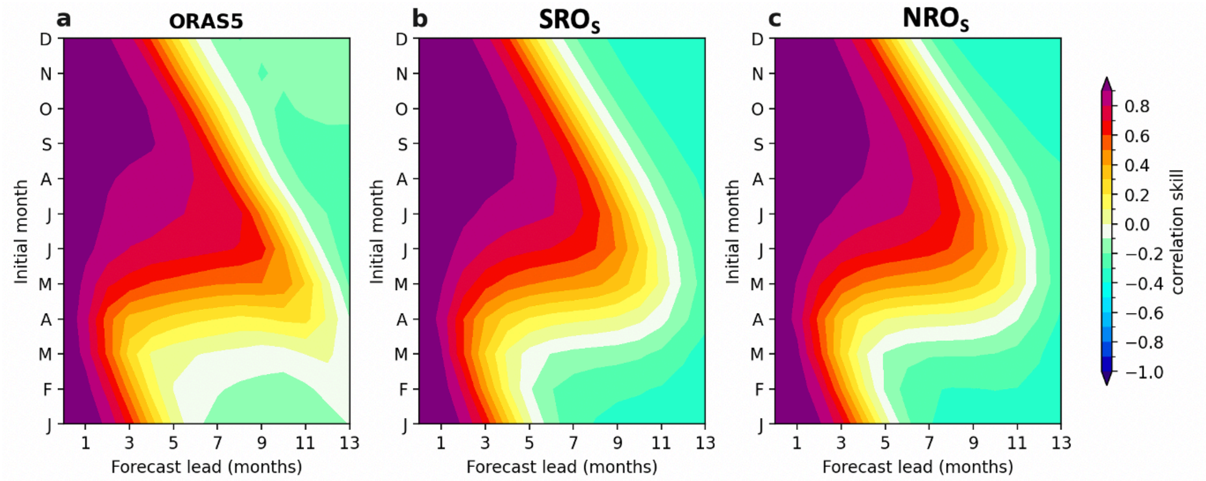

Figure 10: the RO reproduces the ENSO "spring barrier" in predictability. **(a-c)** Persistence of SST anomalies as a function of initial month and forecast lead for ORAS5, and the linear, stochastic, seasonal SRO and nonlinear, stochastic, seasonal NRO fitted to observations. The RO models used in the Figs. 8-12 original analyses are based on equations 4, 5, with *h* defined from the equatorial average heat content. The parameters were obtained from RO fit to observations or CMIP (see Table 2 for details and observed coefficient values). The stochastic forcing uses red noise for ξ_T; ξ_h, whose amplitude and ~1 month decorrelation are estimated based on residuals of the fit. Panel b is based on the seasonal SRO (i.e. *R(t)* as on Fig. 9 and *b*=*B*=*c*=0) and c on the seasonal NRO (i.e. *R(t)* as on Fig. 9 and *b*, *B*, *c* as in Table 2).

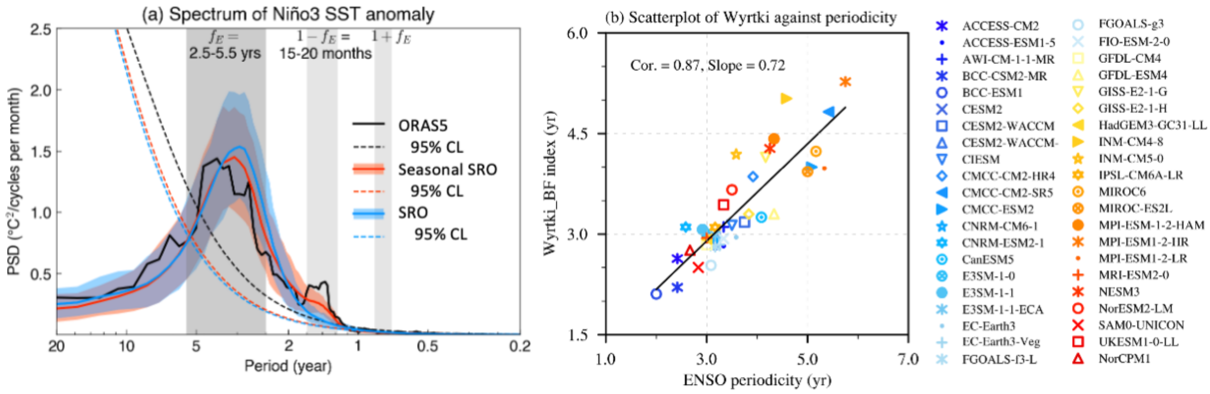

Figure 11: the RO reproduces ENSO dominant timescales. **(a)** Multi-taper power spectral density (PSD) of the normalized Niño3 indices for ORAS5 (1958-2022, black curve), SRO model (red curve) and seasonal SRO model (blue curve). 100 members (65yr each) are generated based on each model and the shading denotes 10%-90% quartile range. The dashed curves indicate the 95% confidence level (CL) calculated from the 95th percentile of an AR(1) process. The grey shading represents the approximate frequency range of ENSO (f_E) and the near-annual combination tones (1-f_E and 1 + f_E), where 1 corresponds to the annual frequency. **(b)** Scatterplot of the approximate Wyrtki index period $2\pi/(F_1F_2)^{1/2}$ against ENSO periodicity (estimated as on Fig. 2g) in 42 CMIP6 historical simulations (1920-1999). The linear regression fit is indicated by the black line (correlation coefficient and slope on the top left). The RO models used in the Figs. 8-12 original analyses are based on equations 4, 5, with *h* defined from the equatorial average heat content. The parameters were obtained from RO fit to observations or CMIP6 (see Table 2 for details and observed coefficient values). The stochastic forcing uses red noise for ξ_T; ξ_h, whose amplitude and ~1 month decorrelation are estimated based on residuals of the fit. Figure 11a analyses use the SRO (*b*=*B*=*c*=0, with a constant *R* for the SRO and R(t) as on Figure 9 for the seasonal SRO).

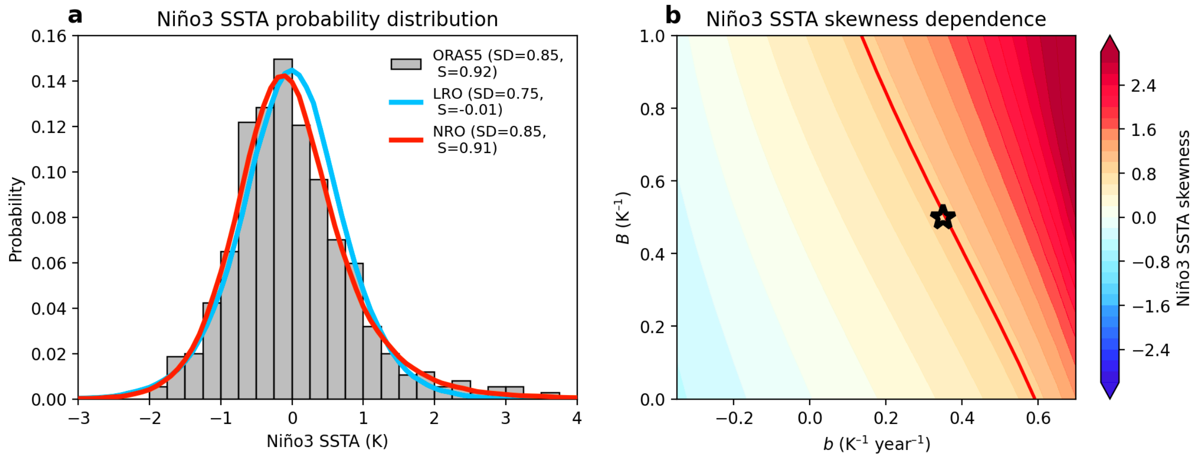

Figure 12: the RO reproduces ENSO amplitude asymmetry. **(a)** Probability distribution of Nino3 SSTA for the observation (ORAS5, gray bars), and of the *T* variable from 20000 years simulations with the stochastic linear (blue) and nonlinear (red) RO models. The standard deviation (SD) and skewness (K) of *T* are indicated in the legend. **(b)** *T* skewness as a function of state-dependent noise forcing amplitude (*B*) and quadratic nonlinearity (*b*). The red curve indicates the observed level of skewness. The black star indicates the parameters of the NRO used in panel (a). The RO models used in the Figs. 8-12 original analyses are based on equations 4, 5, with *h* defined from the equatorial average heat content. The parameters were obtained from a RO fit to observations (see Table 2 for details and coefficient values). The stochastic forcing uses red noise for ξ_T; ξ_h, whose amplitude and ~1 month decorrelation are estimated based on residuals of the fit. Figure 12 analyses use the SRO (*b*=*B*=*c*=0) and NRO (*b*, *c* obtained from the fit as in Table 2; *B* set to a 0.5 K^{-1} value in order to match the observed ENSO skewness, which compares well with observed estimates of 0.3 from Levine et al. 2017 or 0.1-0.5 from Kug et al. 2008), with a constant *R* in both cases.

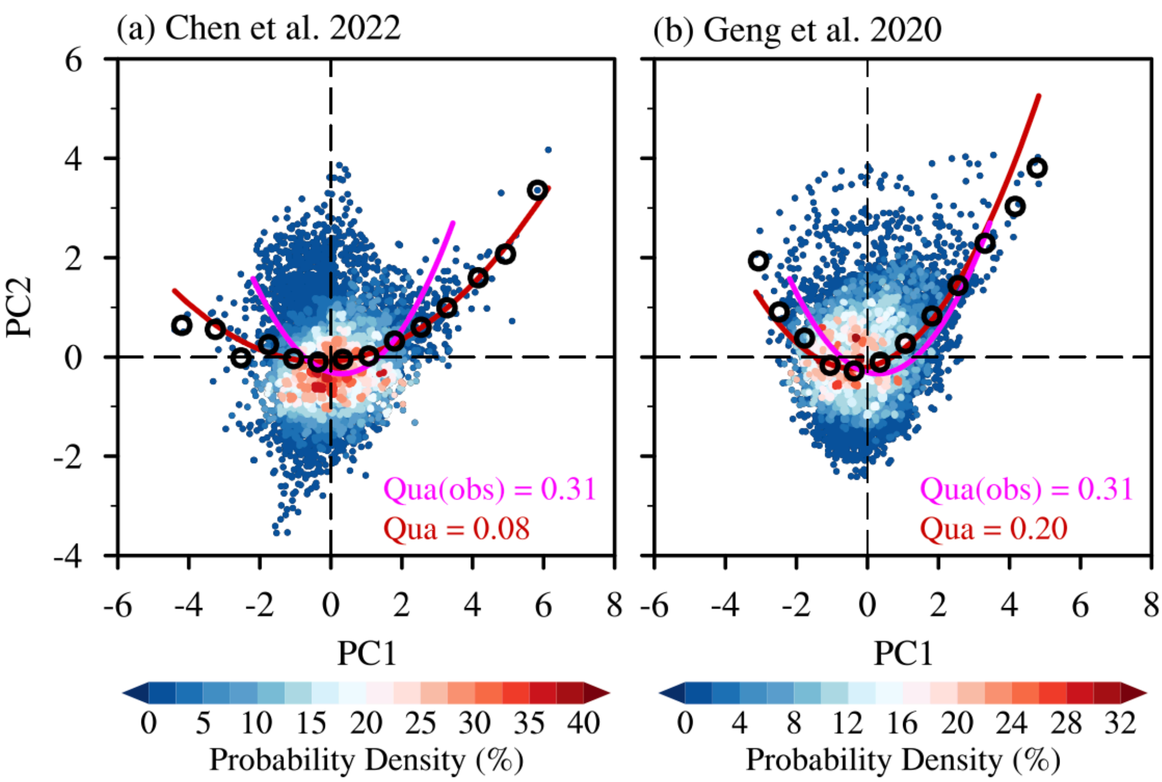

Figure 13. RO extensions can reproduce ENSO pattern diversity. Figure similar to Figure 3c (scatterplot between the first and second normalized principal components PC1 and PC2 of the tropical Pacific SST anomalies in observations), but here for 500-years simulations with two different extensions of the NRO with two SST variables: **(a)** Chen et al. (2022), **(b)** Geng et al. (2020). Having two variables for SST variations T_E in the eastern (Niño3) and T_C in the central-western (Niño4) equatorial Pacific allows addressing ENSO diversity: equivalent values to PC1,2 in observations are obtained from a linear combination of their T_E, T_C time series as in Takahashi et al. (2011). The shading displays a kernel density estimate of the joint PC1, PC2 probability distribution, but it is replaced by a conventional scatterplot below a given threshold. Black hollow circles represent the median PC2 value in 0.75-wide PC1 bins. Quadratic fits to the PC1,PC2 distribution are plotted in red, with the quadratic coefficient value indicated on each panel. The quadratic fit obtained from observed values on Fig. 3c is plotted in magenta on both panels.

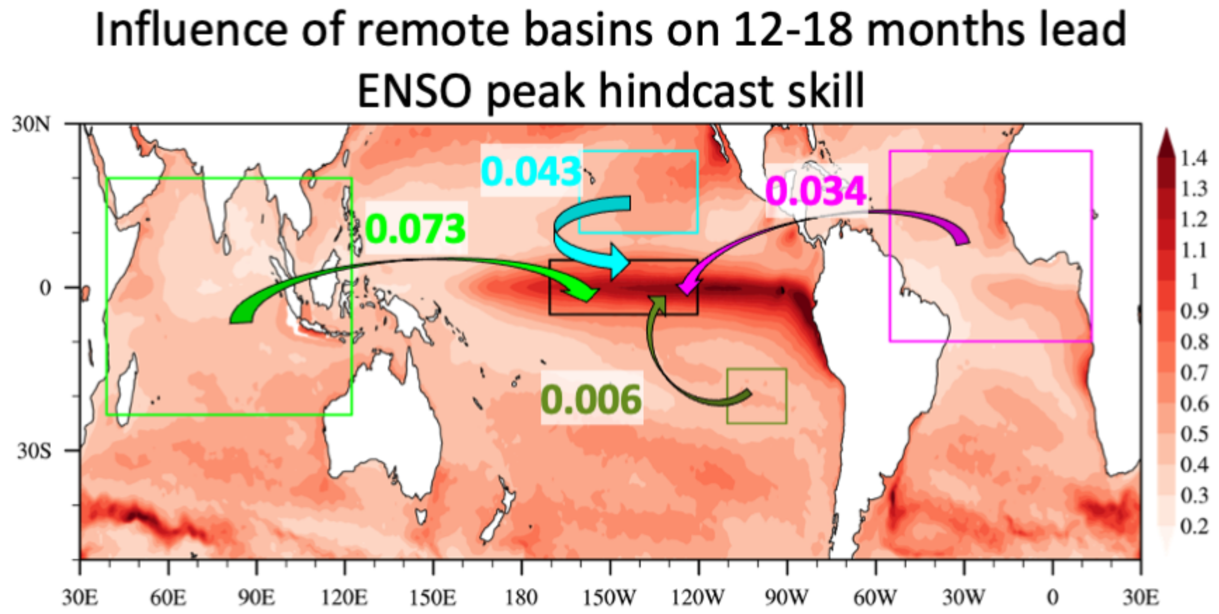

Figure 14. Extended recharge oscillator (XRO) estimate of the influence of remote basins on the 12-18 months lead ENSO peak hindcast skill. Map of the observed standard deviation of SST anomalies since 1980. The frames delineate the tropical Indian Ocean (light green), tropical north Atlantic (magenta), and the center of actions of the North (light blue) and South (dark green) Pacific Meridional Modes (NPMM and SPMM, respectively). The ENSO peak (Niño3.4 November-January average SST anomalies) 12-18 months lead correlation skill increases from accounting for the initial conditions of each mode is indicated by the arrows in the matching color, following the methodology of Zhao et al. (2024) and similar to their Figure 3. The increased predictability is estimated from a NRO coupled to simple representations of various climate modes in each basin that are driven by stochastic and ENSO remote forcing and are feeding back on ENSO. The Indian Ocean contributes most to the skill increase, followed by the NPMM and tropical North Atlantic. The SPMM has only a weak influence on ENSO predictability. Note that those numbers are indicative, , since they vary seasonally and are dependent on the target ENSO phase and RO dynamics details. They however illustrate the usefulness of the RO for studying ENSO interactions with regions outside the tropical Pacific.

Parameter	Name	Associated processes
R	Bjerknes feedback	Thermal damping by surface heat fluxes (clouds, evaporation) Damping by mean circulation Thermocline feedback Advective feedbacks
F_1	Delayed oceanic feedback efficiency	Delayed thermocline feedback Delayed advective feedback
ε	Basin adjustment	Oceanic waves and efficiency of boundary reflections
F_2	Recharge/discharge efficiency	Sverdrup transport Eastern boundary reflection Meridional wind structure
$\sigma_{T,h}$	Stochastic forcing amplitude	Westerly-wind burst (WWBs), short-term atmospheric variability unrelated to ENSO and the associated heat and momentum fluxes
B	Stochastic nonlinearity Multiplicative noise efficiency	Westerly-wind bursts modulation by ENSO ("multiplicative noise"): the tendency for more, stronger WWBs during El Niño than during La Niña
b	Deterministic quadratic nonlinearities	Atmosphere • Asymmetry in atmospheric convective response to warm versus cold SST anomalies Ocean • Tropical Instability Waves (TIWs) • Nonlinear Dynamical Heating • Thermocline feedback nonlinearity
c	Deterministic cubic nonlinearities	?

Table 1. ***RO parameters naming conventions and associated processes***. Various parameters of the RO equations 4,5, the naming conventions used in this paper for each parameter, and the processes underlying the associated term in the equation.

Parameters	SRO	NRO
$R\ (year^{-1})$	-1.13	-1.13
$F_1\ (\mathrm{K\,m^{-1}\,year^{-1}})$	0.19	0.19
$\varepsilon\ (year^{-1})$	0.38	0.38
$F_2\ (m\ \mathrm{K^{-1}\,year^{-1}})$	17.58	17.58
$\sigma_T\ (\mathrm{K\,year^{-1}})$	2.22	2.22
$\sigma_h\ (m\ \mathrm{year^{-1}})$	14.37	14.37
$b\ (\mathrm{K^{-1}\,year^{-1}})$	0.	0.35
$c\ (\mathrm{K^{-1}\,year^{-1}})$	0.	-0.04
$B\ (\mathrm{K^{-1}})$	0.	0.5

Table 2. ***Parameter values for the original RO analyses in this review***. Various stochastic RO (SRO) and nonlinear RO (NRO) simulations were used for the Figures 8 to 12 original analyses in this review. This table provides parameter values obtained from a fit to *h, T* 1958-2020 ORAS5 oceanic reanalysis (Zuo et al. 2019) with *h* defined as the 5°N to 5°S, 120°E to 80°W average 20°C isotherm depth anomalies, and T as Niño3 (5°N to 5°S, 150°W to 90°W) SST anomalies. All parameters but B are obtained from a nonlinear fit of equations 4, 5 to these observations. The stochastic forcing uses red noise for ξ_T; ξ_h, whose amplitude and ~1 month decorrelation timescales (13.27 year^{-1} for *T* and 10.83 year^{-1} for *h*) are estimated based on residuals of the fit. *B* is set to the value for which the *T* skewness matches the observed value (see Figure 12). SRO simulations set all the values of the nonlinear coefficients *b, B, c* to zero. NRO simulations use at least one nonzero value for these coefficients. Seasonal SRO or NRO simulations have seasonally varying coefficient values (see, e.g. *R(t)* as a blue curve on Figure 9a,b). A similar procedure is applied to 1958-2020 CMIP6 historical simulations is applied to obtain coefficient values in CMIP6 models.

	Mean state	ENSO
Observed trends	Walker cell intensification Stronger zonal SST gradient	More extreme El Niño events?
Climate models	Walker cell slowdown Weaker zonal SST gradient	More extreme El Niño events in models that can reproduce them
RO	No theory for mean state No complete recipe for RO parameters dependency on mean state	RO not successful in explaining ENSO changes in models Need for a RO that resolves diversity and/or extreme events?

Table 3. ***Tropical Pacific response to anthropogenic forcing summary***. This table summarizes the section 5.3 reviews of the tropical Pacific mean state (left column) and ENSO (right column) response to anthropogenic forcing over recent decades in observations (first line), in climate models future projections (second line). The bottom line summarizes the current RO status in view of the mean state and ENSO response to anthropogenic forcing.